Current Biology

Volume 22
Number 10

May 22, 2012

www.cellpress.com

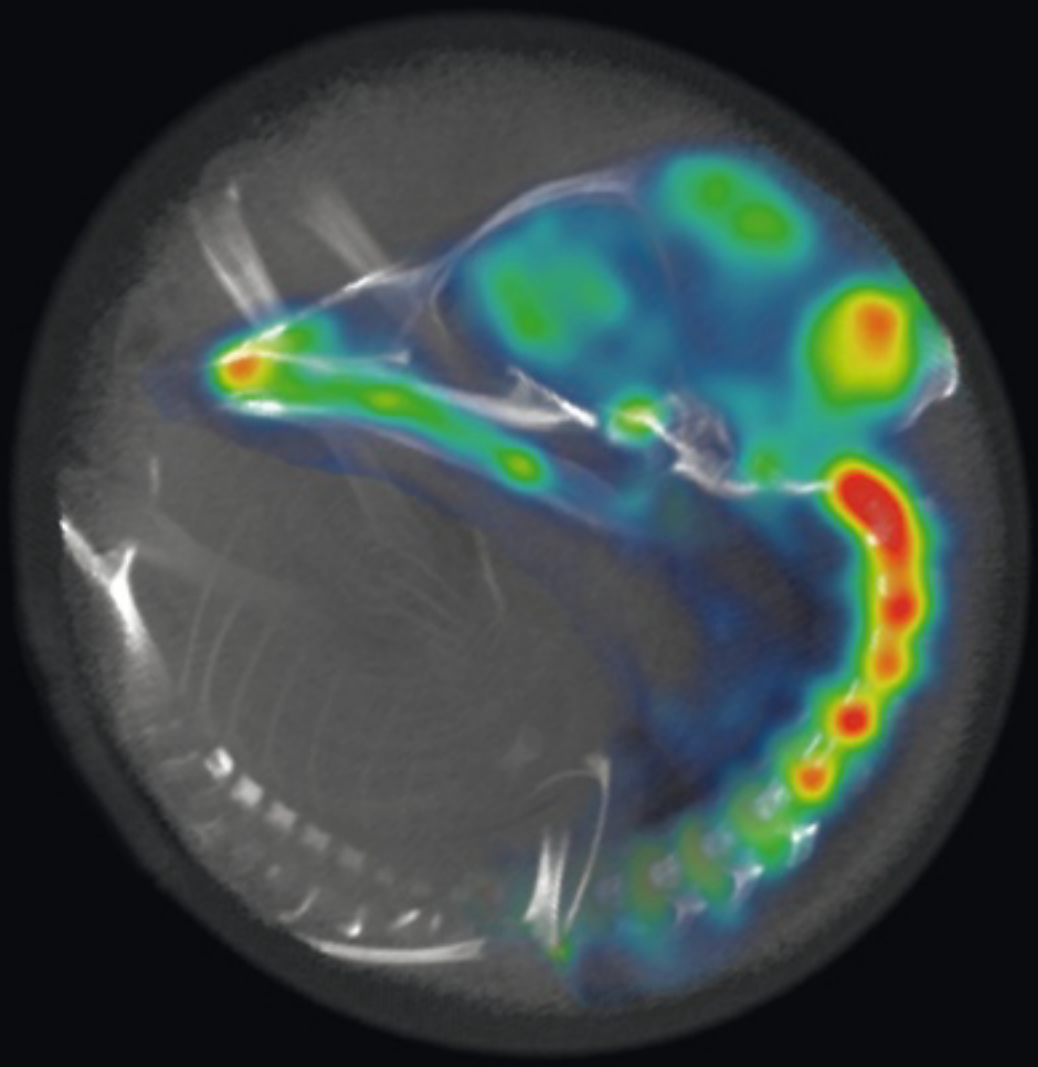

Awakening the Embryonic Brain

On the cover: An X-ray computed tomography image of the chicken embryo skeleton inside an egg, which shows the developmental stage, together with a positron emission tomography image showing nervous system activity in the brain. In this issue, Balaban et al. (pages 852–861) report that the activity in chicken embryo brains is inversely related to behavioral activity, with different sleep-like states emerging for the first time. Playing meaningful sounds selectively induced patterns of embryonic brain activity similar to awake, posthatching animals. Image 3D rendering by Carmen García-Villalba.

Current Biology 22, 852–861, May 22, 2012 ©2012 Elsevier Ltd All rights reserved DOI 10.1016/j.cub.2012.03.030

Article

Waking-like Brain Function in Embryos

Evan Balaban,[1,2,3,*] Manuel Desco,[1,4] and Juan-José Vaquero[1,4]
[1]Unidad de Medicina y Cirugía Experimental, Hospital General Universitario Gregorio Marañón, 28007 Madrid, Spain
[2]Scuola Internazionale Superiore di Studi Avanzati, 34136 Trieste, Italy
[3]Behavioral Neurosciences Program, McGill University, Montreal, QC H3A 1B1, Canada
[4]Departamento de Bioingeniería e Ingeniería Aeroespacial, Universidad Carlos III de Madrid, 28911 Madrid, Spain

Summary

Background: Experience-dependent plastic changes in the brain underlying complex forms of learning are generally initiated when organisms are awake, and this may limit the earliest developmental time at which learning about external events can take place. It is not known whether waking-like brain function is present prenatally in higher vertebrate (bird or mammal) embryos, or whether embryos have brain circuitry that can selectively turn on a waking-like state in response to salient external sensory stimulation.
Results: Combining submillimeter-resolution brain positron emission tomography (PET), structural X-ray computed tomography (CT) of the skeleton for fine-scale embryo aging, and noninvasive behavioral recording of chicken embryos in the egg revealed unexpectedly wide variation in prenatal brain activity, inversely related to behavioral activity, which developed into different sleep-like fetal brain states. Brief prenatal exposure to a salient chicken vocalization (eliciting strong postnatal behavioral responses) increased higher-brain activity significantly more than a spectrally and temporally matching "nonvocal" noise analog. Patterns of correlated activity between the brainstem and higher-brain areas resembling awake, posthatching animals were seen exclusively in chicken-stimulated embryos.
Conclusions: Waking-like brain function is present in a latent but inducible state during the final 20% of embryonic life, selectively modulated by context-dependent monitoring circuitry. These data also reveal the developmental emergence of sleep-like behavior and its linkage to metabolic brain states and highlight problems with assigning embryo brain states based on behavioral observations.

Introduction

Adult bird and mammalian nervous systems cycle through three functionally distinct brain states on a daily basis: non-rapid eye movement (NREM or slow-wave) sleep, rapid eye movement (REM or paradoxical) sleep, and waking [1, 2]. Classically defined using whole-brain electroencephalographic (EEG) changes and behavior [3], these states also differ in brain metabolic and gene expression patterns [4, 5], as well as in the organism's responsiveness to environmental perturbations (lower in sleep than in waking). However, presentation of a salient sound like a human subject's own name during NREM sleep elicits waking at lower sound levels [6] and selective enhancement of brain activation [7, 8], as compared to stimulation with other names or tones, demonstrating selective monitoring circuitry that operates during nonwaking states. An organism's ability to exhibit complex forms of learning about external events is generally limited to waking periods [1, 3].

Although it is customary to assign human prenatal brain states using behavioral observations made with ultrasound sonography [9], the richest source of combined behavioral and neural measurements comes from invasive EEG studies in fetal sheep and chickens, species with grossly similar patterns of EEG and behavioral development [10]. In both species, waking (defined as an open-eyed vigilant state with a desynchronized EEG pattern) occurs only after birth [11–16]. Embryos spontaneously alternate between a high-amplitude EEG state (reminiscent of NREM sleep after birth) and a low-amplitude EEG state (reminiscent of REM sleep after birth), emerging by 80%–90% of embryonic development [10, 17–19]. Behavioral or EEG changes in response to environmental stimulation first appear late in embryonic development in both species [19–26]. In sheep, late-term fetal stimulation with an artificial voice-like sound causes EEG changes that appear to be qualitatively similar to brief periods of arousal from a sleeping state in postnatal animals [27–29]; it is unknown whether prenatal brains exhibit selective monitoring circuitry similar to adults.

To better determine whether prenatal brains have waking-like states and selective monitoring circuitry, we developed a minimally invasive procedure that does not interfere with normal development and can simultaneously monitor neural activity everywhere in the brain with equal sensitivity. We applied submillimeter spatial resolution positron emission tomography (PET) to chicken embryos during the last 30% of their embryonic development, using cellular uptake of 2-deoxy-2-[^{18}F]fluoro-D-glucose (^{18}FDG) to measure brain metabolic activity ([30]; see Figure S1A available online). Skeletal characteristics measured by X-ray computed tomography (CT, [31]) were used to assign developmental stages according to conventional embryological standards [32]. Continuous recordings of cardiac activity, movements, and emitted sounds were obtained from vibrations recorded from the eggshell [33] to quantitatively measure the relationship between embryonic brain activity and behavior (Figures S1B and S1C). Selective monitoring circuitry was assessed by comparing embryos maintained in silence with those exposed to a well-characterized chicken vocalization (highly behaviorally significant after birth [34, 35]), or to a well-controlled "filtered noise" sound (synthesized from this same stimulus and similar in spectral and temporal characteristics, but with a nonvocal timbre; Figure S1D). We found waking-like brain function present in a latent but inducible state during the final 20% of embryonic life, and functional evidence of selective monitoring circuitry that induces changes in prenatal brain states.

Results

Characterizing Variation in Embryo Brain Activity Patterns

Embryo brains did not exhibit a spatially uniform pattern of brain metabolic activity (Figure 1A). Activity levels were

*Correspondence: evan.balaban@mcgill.ca

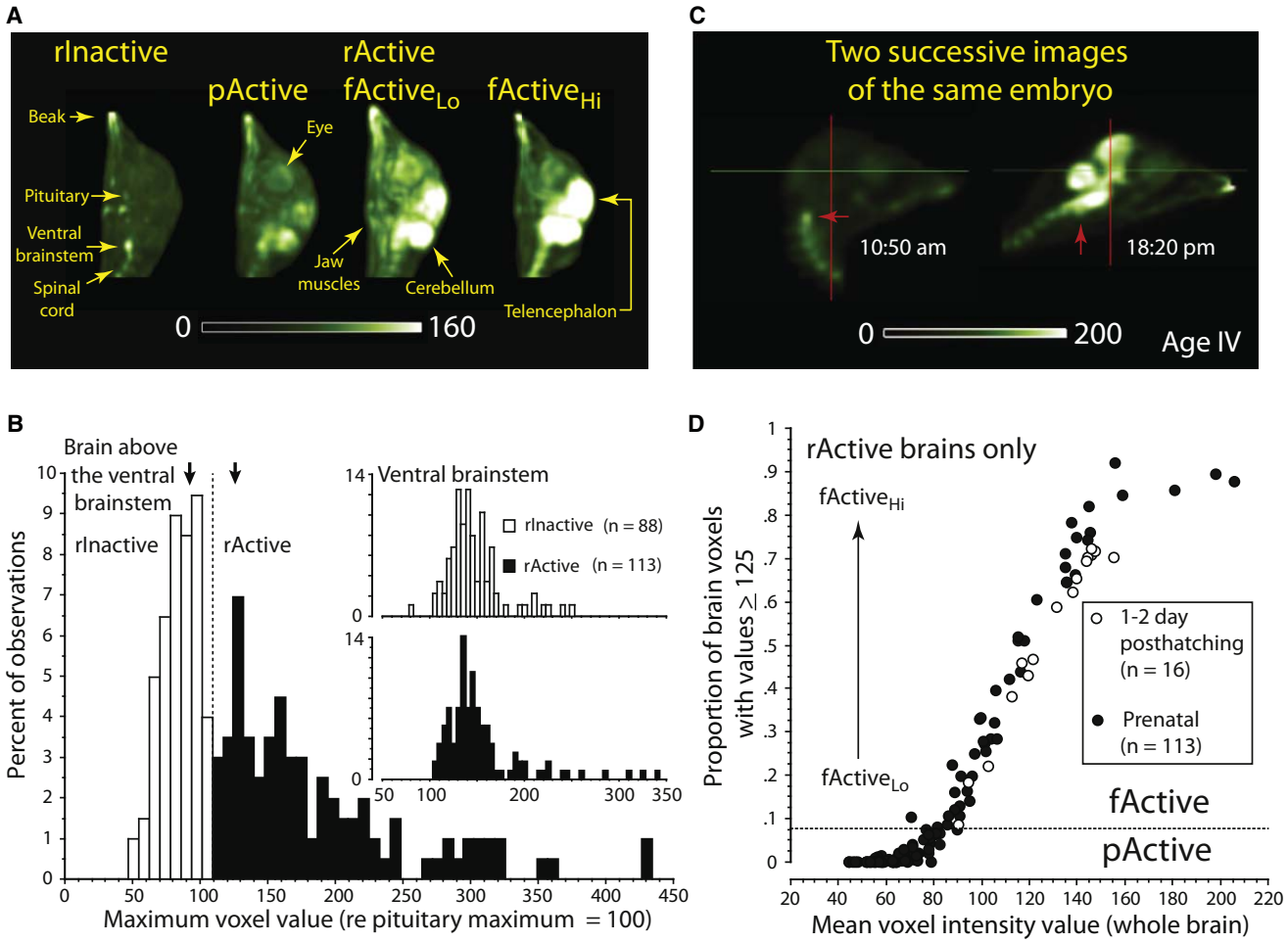

Figure 1. Defining Embryo Brain Metabolic Patterns

(A) Activity patterns seen across all developmental stages and experimental conditions. Each PET image is a sagittal maximum intensity projection of the head of a single subject (beak upward, dorsal to the right). The scale bar indicates the dynamic range of image intensities (normalized to the maximum value in the pituitary = 100). rInactive, brains with maximum activity above the brainstem in the range of the white bars in (B); rActive, brains with maximum activity above the brainstem in the range of the black bars in (B). pActive, fActive$_{Lo}$, and fActive$_{Hi}$ are illustrated in (D).

(B) Histogram of the maximum volume element (voxel) values in the higher brain; arrows indicate the first two peaks of the distribution. The vertical line between them at x = 108 separates rInactive (white) from rActive (black) embryos. Inset: histogram of maximum voxel values in the ventral brainstem for rInactive (upper graph, white) and rActive (lower graph, black) embryos; Mann-Whitney test, n = 88 and 113, p > 0.5.

(C) Images from successive sessions within the same day for a single subject (times indicated, scale bar as in A). The earlier session was silent; the later session included a 2 min exposure to the chicken sound. Red arrows indicate the same structure in the ventral brainstem.

(D) The proportion of all brain voxels with values ≥ 125 (normalized units) versus mean voxel intensity over the whole brain for 113 rActive embryos (black circles) and 16 posthatching birds (white circles). Correlation: r = 0.95, n = 129, p < 0.0001.

consistently high in the spinal cord and brainstem but varied widely in all other brain structures, including the cerebellum, midbrain, hypothalamus, thalamus, and forebrain. Of the 201 embryos studied here, 58% had relatively high metabolic activity in the ventral brainstem (reflecting its important role in regulating basic physiological functions), but not anywhere else in the brain (Figure 1A); the other 42% had even stronger activity in higher-brain areas (dorsal and rostral to ["above"] the ventral brainstem), presumably related to more complex functions that become important leading up to and after hatching. To capture these coarse pattern differences, we classified embryos into "relatively inactive" (rInactive) and "relatively active" (rActive) categories, according to their higher-brain activity (Figure 1B). These categories did not simply reflect random variation between embryos, because single embryos could shift their patterns on successive imaging sessions within the same day (Figure 1C). The spatial distribution of higher-brain activity among embryos was also nonrandom; maximum activity in two higher-brain regions was strongly correlated (cerebellum and forebrain, r = 0.96, n = 201, p < 0.0001, Figure S2A; these two regions contained the maximum activity above the ventral brainstem in 88% of all embryos). Ventral brainstem activity was statistically independent of higher-brain metabolic patterns (Figure 1B, inset). Thus, activity in higher-brain circuits was regulated in a unitary way, independent of ventral brainstem levels.

Embryo brains in the rActive group were further subdivided with a second classification based on posthatching brain function. This procedure used data from 16 awake, sound-exposed, 1- to 2-day-old postnatal chickens, quantifying the proportion of each brain that had metabolic activity above a standard, medium-threshold value (Figure 1D). Embryos with

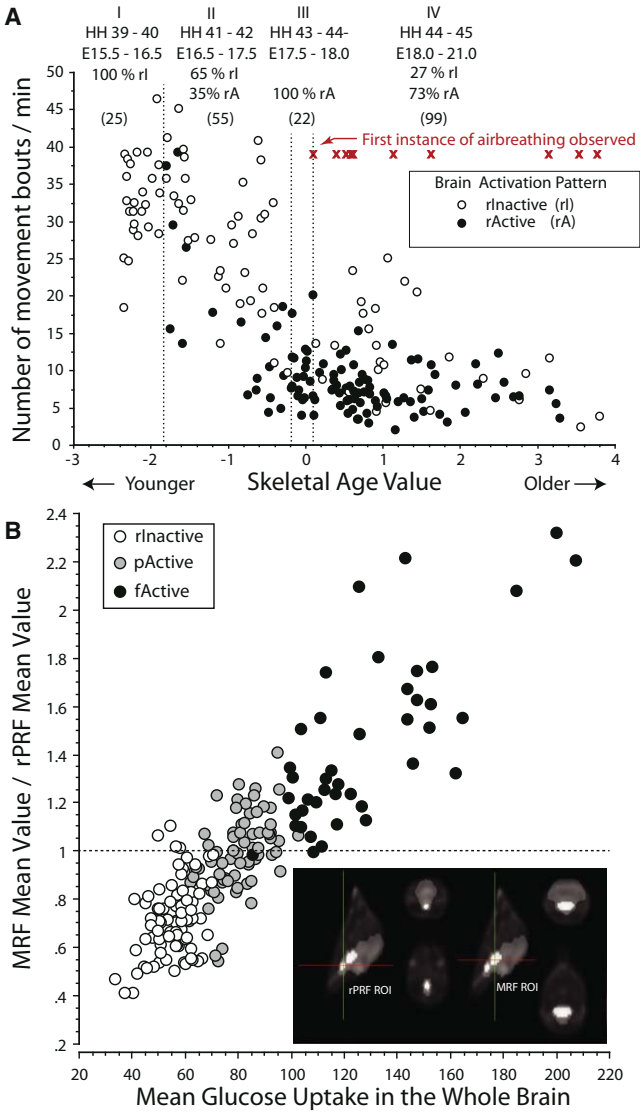

Figure 2. Behavior and Brain Activation Patterns Change as a Function of Developmental Stage and Reticular Formation Activity

(A) Embryo movement activity changes with relative skeletal age ($r = -0.75$, $n = 201$, $p < 0.0001$). Skeletal age values were determined from CT images of each skeleton and are expressed in units relative to the middle of the range of ages studied here, which is defined as 0. Dotted vertical lines separate developmental ranges of interest (see text); the equivalent classical developmental stages [32] and embryonic days of incubation (E) are also given. Red "x"s indicate internally pipped embryos; sample sizes are given in parentheses. Percentages indicate the proportion of embryos with rInactive (rI) and rActive (rA) brain patterns.

(B) Reticular activation ratios versus mean metabolic activity over the whole brain for rInactive (white circles), pActive (gray circles), and fActive (black circles) embryos; correlation: $r = 0.88$, $p > 0.0001$, $n = 201$. Regions of interest (ROIs) are shown in the inset. Means ± SEM: rInactive, 0.72 ± 0.02 (n = 88); pActive, 0.99 ± 0.02 (n = 71); fActive, 1.44 ± 0.06 (n = 42); Kruskal-Wallis test: $H = 133.7$, $df = 2$, $p < 0.0001$; all groups significantly different from each other. The relationship between reticular activation ratios and movement was also significant [number of movements per minute = $-9.90 + 22.58/(MRF/rPRF)$, $r^2 = 0.54$, $F(1,199) = 237.0$, $p < 0.0001$].

rActive brains that had proportions greater than or equal to the lowest proportion shown by any awake posthatching chick were designated "fully active" (fActive, fA), and those with proportions below this threshold were "partially active" (pActive, pA) (see examples in Figure 1A). In spite of large differences in overall brain activity levels among rInactive, pActive, and fActive embryos, regions with the greatest activity were similar throughout the developmental period studied here (Figure S2B). These data are most consistent with a switching mechanism that modulates a common, global spatial pattern of brain activity.

Changes in Higher-Brain Activation Follow a Developmental Pattern

Embryos were developmentally ordered using a principal component analysis of the volume of a set of basal cranial bones plotted against the volume of the rostral vertebral column, measured from each individual's CT image. The first principal component, which accounted for 98.5% of the variation among individuals and agreed with traditional morphological measures of developmental stages ([32]; see the Supplemental Experimental Procedures), was used to quantify developmental stage ("skeletal age"). Embryos displayed increasing probabilities of higher-brain activation and decreasing movement frequencies as development proceeded (Figure 2A). Combining brain and behavioral information, we noted four time periods of interest. Early on (Age I, embryonic day (E) 15.5–16.5, stage 39-40 [32], 74%–79% of the 21-day incubation period [ip]), embryos exhibited relatively high rates of movement with no higher-brain metabolic activation. This was followed by the first appearance of higher-brain activation (Age II, E16.5–17.5, stage 41-42, 80%–83% ip), with decreasing movement rates as development proceeded. Toward the end of this phase, there was a relatively short period (Age III, E17.5–18.0, stage 43-44$_{minus}$, 83%–86% ip) where all embryos had higher-brain activation. Finally, there was a prolonged period before hatching that contained both rInactive and rActive brain patterns with low levels of movement (Age IV, E18.0–21.0, stage 44-45, 87%–100% ip); the beginning of this period coincided with the first signs of the transition to air breathing (self-puncture of the chorioallantoic membrane [internal pipping]). The proportion of embryos with higher-brain activity among each of these four periods was significantly different from the other periods (heterogeneity: $G = 86.99$, $df = 3$, $p < 1.0 \times 10^{-5}$, all groups different at the $p < 0.01$ level), indicating that these changes represent a developmental pattern rather than random sampling variation. In subsequent analyses, Ages II and III were combined to improve statistical power, based on the high similarity of their brain activation pattern maxima (Figure S2B), and because Age III appears to represent the culmination of trends starting in Age II that peak in the population during a brief period just prior to the transition to air breathing.

Changes in Reticular Formation Activity Are Related to Embryo Higher-Brain States

Cell groups in the pontine and mesencephalic reticular formation importantly regulate postnatal brain states in both birds and mammals [1, 2, 36, 37]. Changes in metabolic activity were therefore compared in regions of interest (ROIs) encompassing the rostral pontine (rPRF) and mesencephalic (MRF) reticular formation of embryos (Figure 2B; ROIs shown in inset). Activity differences in pontine and mesencephalic circuits (expressed as MRF/rPRF, "reticular activation ratio") were significantly related to both brain states and behavioral differences (Figure 2B), demonstrating that the control of metabolically different brain states may be similar in embryos and adults.

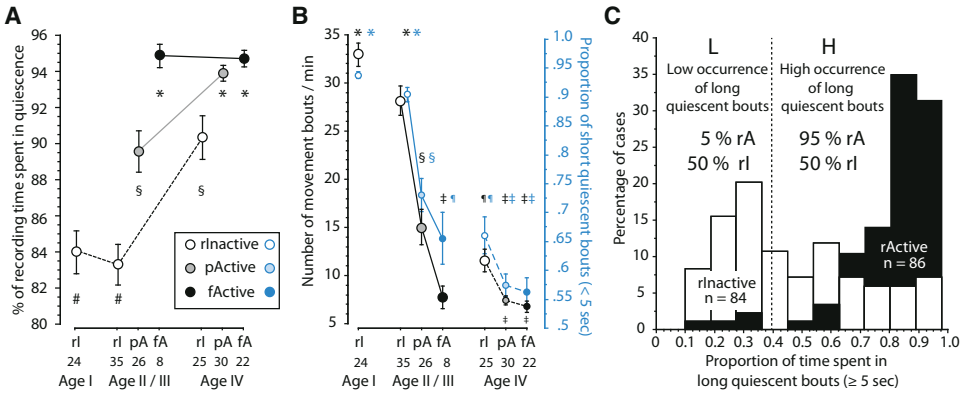

Figure 3. Embryo Brain Activity Is Inversely Related to Movement

(A) The percentage of time that embryos spent in quiescence differed significantly among brain activation patterns (Kruskal-Wallis test: H = 83.14, df = 6, p < 0.0001).

(B) Movement rate (black) changed in parallel with the proportion of short (<5 s) quiescent periods (blue). Correlation among all embryos: r = 0.89, n = 170, p < 0.0001; Kruskal-Wallis tests: movement rate: H = 113.1, df = 6, p < 0.0001; quiescent periods: H = 109.5, df = 6, p < 0.0001. For (A) and (B), all error bars are ±1 SEM. Symbols near each data point (color coded according to variable) indicate the results of post hoc tests corrected for multiple comparisons; points with different symbols are significantly different (p < 0.05). Sample sizes are shown at bottom.

(C) Population histograms showing the proportion of time spent in long (≥5 s) quiescent bouts for rInactive (white) and rActive (black) embryos. These data were also categorized into L and H groups (with low and high occurrences of long quiescent periods, respectively; threshold as indicated by the dotted vertical line). rActive (rA) embryos were significantly more likely to have high occurrences of long quiescent bouts than were rInactive (rI) embryos (G = 49.12, df = 1, p = 2.4 × 10^{-12}).

Higher-Brain Activity Is Inversely Related to Embryo Movement

Higher-brain activity was strongly associated with behavioral inactivity (quiescence). Quiescence increased both as development proceeded and within developmental stages in association with changes in higher-brain activity (Figure 3A). This relationship was specifically linked with the disappearance of short (<5 s) quiescent bouts (Figure 3B). Indeed, embryos with higher-brain activity spent a significantly greater proportion of their time in long (≥5 s) quiescent bouts (mean ± SEM, rActive: 80.0% ± 1.8%, n = 86; rInactive: 46.5% ± 2.6%, n = 84; Mann-Whitney test, z = 7.97, p < 0.0001; Figure 3C).

Is embryo quiescence like sleep? Sleep bout durations are known to follow an exponential distribution in many adult mammals [38], as do quiescent period durations in fetal sheep [16]. Chick embryo movement bout durations for all stages and brain patterns were exponentially distributed (Figure 4A), as in fetal sheep [16] and early postnatal rodents [39, 40]. However, rInactive embryos had power-law quiescent period duration distributions at 70%–80% of embryonic development (Age I); these became indeterminately distributed during Age II/III and exhibited sleep-like exponential distributions at Age IV (Figure 4B). In contrast, pActive embryos always had sleep-like exponential distributions, and fActive embryos always had indeterminate distributions.

Embryo quiescence was related to eye movements in a manner reminiscent of REM sleep. As expected for REM atonia ([3], active eye muscles coupled with inactive body muscles during REM sleep), glucose uptake by the intrinsic (iris) eye muscles and the jaw (mandibular depressor) muscles had oppositely signed, significantly different partial correlations with quiescence (+ eye, − jaw; Figures 4A and 4B). At all ages, intrinsic eye muscle activity was significantly lower in rInactive embryos than in rActive embryos; eye muscle activity was significantly higher in fActive relative to pActive embryos at Age II/III, but not at Age IV.

Together, these observations suggest that the rInactive brain metabolic state initially did not resemble sleep but changed by Age IV to include a prominent sleep-like component with low levels of eye movement. In contrast, the pActive state was dominated by sleep-like behavior, with indications of both REM-like (increased eye movement) and NREM-like (quiescent) periods; the fActive state differed from sleep, with high levels of eye movement and indicators of integrative brain function (see below).

Higher-Brain Activation Is Stimulus Selective

The effects of sound stimulation were analyzed by comparing the brain activation patterns of groups of embryos that were given equivalent individual exposure to the chicken stimulus or its filtered-noise analog, or who were left in silence. These comparisons showed different brain effects depending on when in development sound stimulation was given. At the earliest period (Age I), stimulation did not produce any higher-brain activation (n = 20 stimulated embryos). By Age II/III, chicken stimulation (C) more than doubled the proportion of embryos with higher-brain activation compared to the other two experimental conditions (Figure 5A; pActive + fActive = 70% versus 33% for filtered-noise [FN] stimulation or silence [S], G = 9.06, df = 2, p = 0.011; this was due to an increased proportion of pActive embryos: 57% C versus an average of 23% for FN and S combined, G = 8.04, df = 1, p = 0.005). Chicken stimulation also resulted in higher-brain activation occurring at significantly earlier stages of development than the other conditions (Figure 5B). These results clearly demonstrate selective monitoring circuitry influencing prenatal brain activity states.

At late developmental stages (Age IV), chicken stimulation drove a nonsignificant increase in the proportion of higher-brain activation (Figure 5A; 76% C, 60% FN, 64% S, G = 1.55, df = 2, p = 0.46) but still had a significant advantage in recruiting brains operating at lower global metabolic levels to pActive status (proportion of pActive brains with modal activity values < 70 normalized units, chicken stimulation: 64%;

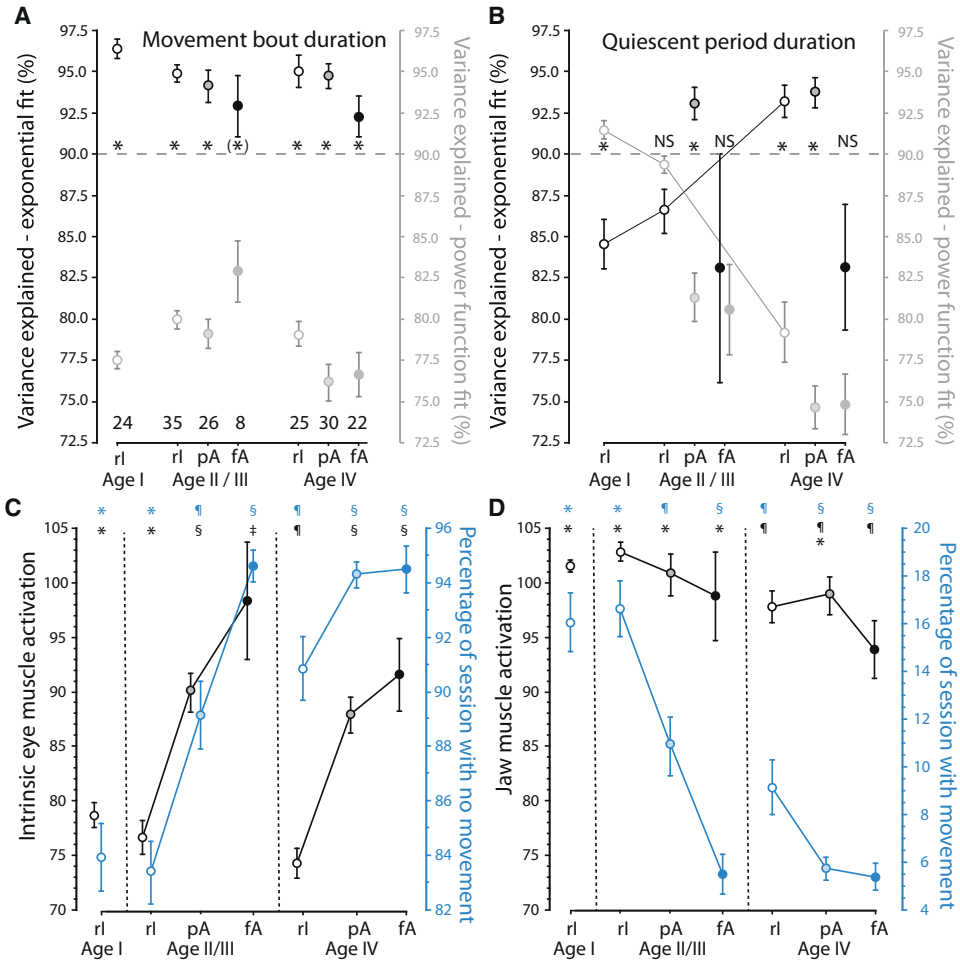

Figure 4. Behavioral and Physiological Measures of Sleep-Like States

(A and B) For movement bout durations (A) and quiescent period durations (B), the mean proportion of variance explained by exponential (black-bordered circles and left y axis) and power function (gray-bordered circles and right y axis) fits are shown for each developmental state/brain pattern (x axis): white-filled circles, rInactive (rI); gray-filled circles, pActive (pA); black-filled circles, fActive (fA). A fit was declared when one function had significantly (*$p < 0.05$) or nearly significantly [(*)$p < 0.06$] better mean fit than the other function and explained an average of >90% of the variance. Error bars are ±1 SEM; sample sizes are shown at bottom of (A).

(C) Mean glucose uptake (normalized units) in the combined right and left intrinsic eye (iris) muscles of individual embryos (black, left y axis) and percentage of the session with no movement (blue, right y axis), versus developmental stage and brain pattern (x axis). Points with the same significance symbol are not significantly different from each other; points with different symbols are significantly different. Error bars are ±1 SEM; sample sizes are as in (A).

(D) Mean glucose uptake in the combined right and left jaw (mandibular depressor) muscles (black, left y axis) and percentage of the session with movement (blue, right y axis) for the same embryos as in (C), versus developmental stage and brain pattern (x axis). Partial correlations with quiescence: eye activity: $r = +0.43$, jaw activity: $r = -0.31$, both $n = 170$, $p < 0.0001$; comparison, $p < 0.0001$. Significance symbols, error bars, and sample sizes are as in (C).

filtered-noise stimulation and silence: 16%, $G = 6.76$, $df = 1$, $p = 0.009$).

The brain effects of stimulation depended on the behavior shown by embryos prior to sound exposure. Individual embryos were classified as having high (H) or low (L) occurrences of long quiescent bouts (as defined in Figure 3C) during the 5 min prior to stimulation (or the equivalent time in embryos maintained in silence). The probability of higher-brain activation was significantly influenced by prior behavior, but the effect of chicken stimulation was not (Figure 5C; log-linear analysis, three-way interaction between stimulus type [chicken or filtered noise and silence combined], brain activity pattern [rInactive or rActive], and prior behavior [low or high occurrence of long quiescent bouts]: $G = 4.40$, $df = 1$, $p = 0.036$). The chicken stimulus on average yielded an additional 25% of higher-brain activations compared to the other two conditions, independent of prior behavior ($G = 17.26$, $df = 2$, $p = 0.0002$).

Only fActive embryos had subtle movement pattern changes as a result of stimulation that significantly differed among the three stimulus conditions (Figure S3A), providing evidence of fActive waking-like function. The behavior and metabolic response patterns of rInactive embryos were also significantly affected by sound stimulation at all developmental stages (Figures S3B and S3C), demonstrating that sound stimulation produced functional changes in rInactive embryo brains, even though it failed to produce higher-brain activation.

Stimulus-Exclusive Induction of Correlated Activity between Brain Areas

An examination of activity relationships between the ventral brainstem, reticular circuits, and higher-brain areas revealed

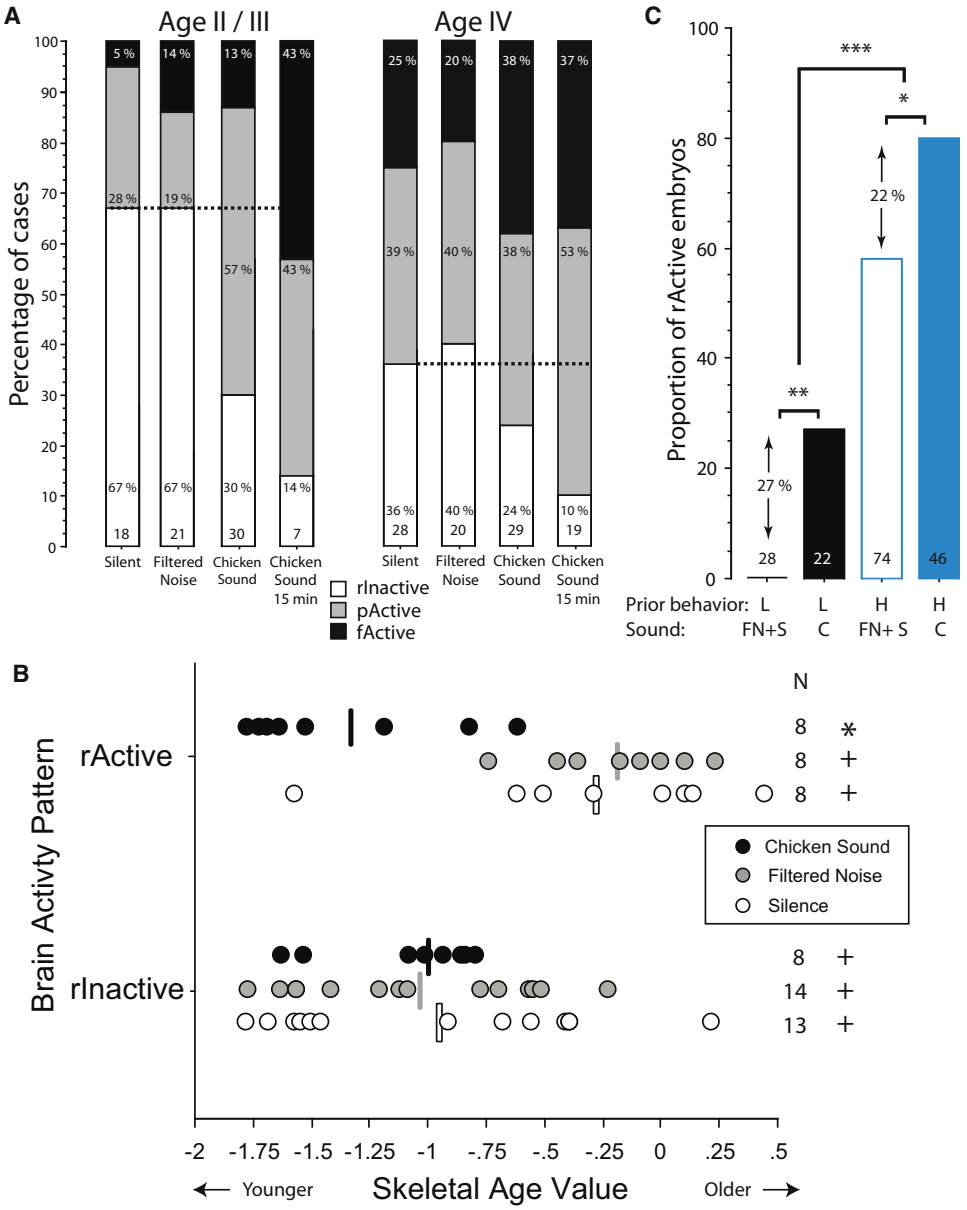

Figure 5. Stimulus-Selective Changes in Brain Activity Patterns

(A) Percentage of embryos with rActive (white), pActive (gray), and fActive (black) brains, arranged by developmental stage and stimulus condition. Age I embryos (n = 25, all rInactive) are not shown; data from embryos stimulated for 15 min are shown for comparison but were not used for statistical analyses. Dotted horizontal lines indicate rInactive silent values; numbers are sample sizes.

(B) Chicken sound exposure developmentally advances higher-brain activation. x axis = skeletal age of individual embryos (see Figure 2A). Vertical bars indicate group means. Skeletal ages were sampled in each condition from the first observed rActive pattern until the first eight rActive embryos were found; rInactive brains served as a control for sampling inequalities. rActive embryos had significant skeletal age heterogeneity among conditions (Kruskal-Wallis test, H = 13.06, df = 2, p = 0.0015, corrected for two comparisons), whereas rInactive embryos did not (H = 0.23, df = 2, p = 0.89). Symbols at right show the results of post hoc tests corrected for multiple comparisons; significantly different groups (p < 0.05) have different symbols.

(C) Proportion of rActive embryos (y axis) as a function of stimulus condition and prior behavior (x axis = low [L] or high [H] occurrences of long quiescent periods [see Figure 3C] during the 5 min preceding stimulation). Stimulus conditions: C, chicken; FN+S, filtered noise and silent conditions combined. *p < 0.05, **p < 0.01, ***p < 0.0001, Fisher's exact tests corrected for multiple comparisons.

developmental changes in brain function unique to chicken-stimulated embryos. Ventral brainstem maximum values and reticular activation ratios were classified into two levels, "normal" (N) and "elevated" (E), based on their distributions (Figure 6A). At Age II/III, the percentage of cases with elevated brainstem values was similar for all embryos with and without higher-brain activation (26% and 23%, respectively). Sound-stimulated embryos had greater brainstem maxima than nonstimulated embryos, independent of higher-brain activity (two-way ANOVA: sound versus silence, H = 4.04, df = 1, p = 0.044; rInactive versus rActive, H = 2.14, df = 1, p = 0.14; interaction, H = 0.55, df = 1, p = 0.46), but chicken-stimulated embryos did not have greater values than filtered-noise-stimulated embryos. In contrast, at the same developmental

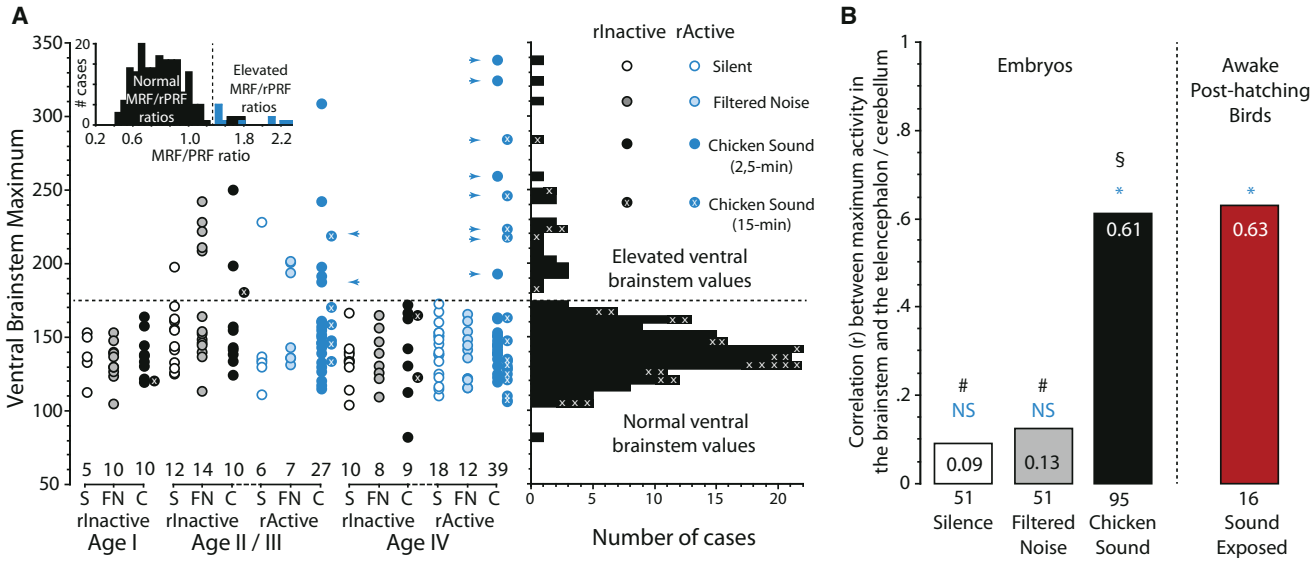

Figure 6. Stimulus-Exclusive Changes in Brain Integrative Function

(A) Left: ventral brainstem maximal activity (y axis) as a function of developmental stage, brain pattern, and sound condition (x axis; C, chicken; FN, filtered noise; S, silence). Right: histogram of the same data. Data points with an "x" are from embryos given 15 min chicken stimulation. Dotted horizontal line at y = 175 separates embryos with normal (lower) and elevated (upper) values. Left inset: histogram for MRF/rPRF ratios of the same embryos, with a vertical dividing line between normal and elevated values at x = 1.5. Only chicken stimulation produced rActive embryos with both elevated brainstem values and MRF/rPRF ratios (blue arrowheads; 10 of 66 rActive C-stimulated embryos versus 0 of 43 rActive S or FN embryos; p = 0.006, Fisher's exact test).
(B) Correlation between maximum values in the brainstem and telencephalon or cerebellum (whichever was higher; 15 min chicken-stimulated birds are included; results do not change without them). Blue symbols: *p < 0.05, corrected for four comparisons; NS, not significantly different from 0. Heterogeneity for the three embryo groups: $\chi^2 = 17.21$, df = 2, p < 0.0001. Black symbols: multiple-comparison-corrected differences among the three embryo correlation coefficients; bars with different symbols are significantly different from each other (p < 0.05). Numbers under the bars are sample sizes.

stages, higher-brain metabolic responses showed a stimulus-selective probability-of-activation difference (Figure 5A). By Age IV, only chicken-stimulated embryos with higher-brain activity showed simultaneously elevated brainstem maxima and reticular activation ratios (Figure 6A, blue arrowheads and blue bars in the inset).

Over all developmental stages, only chicken-stimulated fActive embryos had simultaneously elevated brainstem maxima and reticular activation ratios (Figure 6A, blue arrowheads; see Figure S4 for additional analyses). They also showed a statistically significant correlation between activity in the telencephalon/cerebellum and the ventral brainstem (r = 0.76, n = 10, p = 0.008), seen over all chicken-stimulated embryos and in awake posthatching birds but not seen in either silent or noise-stimulated embryos (Figure 6B; see Figure S5 for further analysis). Thus, prenatal chicken stimulation uniquely produces correlations in the activity of brainstem and higher-brain regions, and chicken-stimulated fActive embryos exclusively have both these correlated activity patterns and the elevated levels of higher-brain activity quantitatively like those seen in awake, posthatching animals.

Discussion

Minimally invasive high-resolution molecular and structural imaging coupled with noninvasive behavioral recording has revealed the prenatal organization of brain metabolic activity patterns and their correspondence to behavior. Like the ability of a person's name to selectively arouse them from slumber, a biologically significant sound can selectively turn on integrated patterns of embryonic brain function reminiscent of waking via a metabolic switching mechanism that regulates higher-brain activity and integrative brain function during the final 20% of embryonic life.

Late-stage embryos go through periods where higher-brain metabolic activity is turned "on" (either spontaneously, via sound stimulation, or by the gentle egg handling necessary for these experiments) and periods where it is turned "off." The "off" state, associated with greater spontaneous movement activity, changes during development from an earlier form not resembling any known, nonpathological adult state to one bearing a resemblance to NREM sleep. From their first appearance, "on" states were associated with a REM-sleep-like behavioral component and had relatively low levels of movement; salient stimuli could drive the appearance of waking-like functional brain characteristics before the initiation of air breathing. Therefore, both a repertoire of distinctive, sleep-like metabolic states and a latent yet inducible whole-brain pattern of organized activity with waking-like characteristics become established in higher vertebrate embryo brains in advance of birth.

In many developing neural circuits, γ-aminobutyric acid (GABA), the major inhibitory neurotransmitter in the adult brain, is initially excitatory [41, 42], and it is known to mediate spontaneous activity in chick embryo spinal cord circuits [43–45]. GABA becomes inhibitory beginning at E14 –E15 in chick embryos [46–48], and this paves the way for increasing control of brainstem and spinal cord circuits by the higher brain. Additional research will be necessary to determine whether the decreases in embryo movement seen here ~1–2 days after the initiation of these cellular changes are a simple consequence of the cellular changes at the systems level or whether the delay indicates a more complex cascade of events relating these two phenomena.

These data may also inform controversies about sleep development in mammals. Some researchers have argued that REM sleep emerges first in development [49], unrelated to early patterns of forebrain activity [50], and is followed by the later emergence of NREM sleep; others have argued that both REM and NREM sleep emerge from a common precursor sleep-like brain state containing a mixture of REM and NREM characteristics [51, 52]. Based on parallel analyses of brain activation patterns, quiescent period distributions, movement, and eye muscle activation recorded in the same individuals, the earliest recognizable metabolic brain state in chick embryos resembling sleep is related to forebrain activation and contains both REM-like and NREM-like periods.

This work also identifies new aspects of the relationship between embryo brain activity and behavior that complicate the assignment of prenatal (and early neonatal) brain states from behavioral data. Embryo movement was greatest when higher-brain regions were metabolically switched off; these movements were presumably under the dominant control of brainstem and spinal cord circuits, which exhibited relatively high metabolic activity. Therefore, larger amounts of movement are not indicative of a REM-sleep-like or waking-like state, and the smaller amounts of movement that occur when higher-brain regions are metabolically switched on can be seen during both sleep-like and waking-like states. Although there may be particular behaviors that occur only during specific brain states, these data underscore the necessity for validating any such candidate behaviors with brain measurements.

The overall probability of different fetal brain states depended on the developmental stage and behavior of embryos, yet as few as seven repetitions of a 2 s sound stimulus over a 2 min period could trigger increased metabolic activity in a coordinated fashion over most of the brain. The chicken stimulus used here induced a significant correlation between activity in the brainstem and higher areas similar to that in awake posthatching animals, and not seen in embryos maintained in silence or exposed to the nonvocal control stimulus. The stimulus-selective monitoring mechanism responsible for these changes operated over a scale of seconds to minutes and was related to activity in pontine and mesencephalic circuits. Continuing work will be necessary to fully map the anatomy, physiology, neurochemistry, and endocrinology of the responsible circuit (or circuits) and to determine the exact relationship between developing brain metabolic patterns and EEG patterns.

An embryological mechanism maintaining higher-brain metabolic activity and the correlation in activity between brain areas in a reduced state, while allowing their upregulation by particular, salient stimuli, has significant implications for our understanding of brain-wide aspects of experience-dependent plasticity and integrated brain function during late prenatal and early postnatal life. High levels of whole-brain metabolic activity are energetically expensive and may pose a danger just as the embryo makes the transition to air breathing because of ischemic risks due to hypoxia [10], which may explain the reappearance of relatively inactive higher-brain states as breathing begins (Age III-IV transition; Figure 2A). A global downregulatory mechanism may also play a more prolonged role by protecting embryo brains from the disruptive effects of external sensory stimulation on neural circuit formation; the time when these protective mechanisms turn off may in part define the start of sensitive or critical periods [53]. By regulating the developmental timing and the circumstances under which the integrative, whole-brain activity that complex forms of learning depend upon is switched on and off, the mechanism that selectively wakes up embryo brains can importantly shape when and how external information affects neural circuitry. This has broader significance in two different ways. First, it may explain stimulus-selective forms of early learning, in which fetuses and/or neonates spontaneously exhibit complex learning about particular classes of stimuli (such as human infants rapidly learning the detailed characteristics of speech sounds). Second, there may be negative developmental consequences if biologically significant stimuli can prematurely wake up and start changing fetal brains before the completion of intrinsic brain circuit development. The mechanism revealed here may lead to a better understanding of postnatal consequences of stimulating the fetal brains of prematurely born infants, and ways to ameliorate any negative consequences of such stimulation.

Experimental Procedures

All animal care and experimental procedures were approved by the local animal use committee. Commercially obtained chicken eggs were incubated for 15–21 days (stages 39–45 [32]) in a light-tight incubator at 37.5°C and 55% humidity and were removed singly in a light-tight container for behavioral recording and imaging. Under a red photographic safelight, a small (4–5 mm diameter) hole was gently cut in the shell overlying the airspace at the blunt end of the egg, where a warm (37.5°C) tracer solution containing ~1.5 mCi of 2-deoxy-2-[^{18}F]fluoro-D-glucose (^{18}FDG) was gently deposited directly onto the region of the intact shell membrane immediately under the hole. A piece of porous wound-closure tape was used to cover the hole, and the egg was placed on a movement-recording device atop a vibration-isolation platform inside a dark, light-tight 37.5°C sound-isolated chamber for the 20 min recording period prior to imaging. Because of the high physiological clearance rate of glucose and the half-life of ^{18}F, the vast majority of ^{18}FDG had been cleared from the bloodstream and was in body tissues by the end of the recording period; further cellular incorporation of any remaining glucose would have little effect on PET image intensities. The PET images therefore represented glucose uptake by cells during the recording period.

From the continuous recordings of embryo behavior and cardiac physiology ([33], voltage deflections), a movement bout was defined as any voltage deflection greater than the heartbeat that was separated by more than 150 ms from any other such deflection; quiescent (inactive) periods were defined by the absence of voltage deflections above the level of the heartbeat. After 10 or 13 min of silence, some embryos were stimulated with either 5 or 2 min (respectively) of the chicken or filtered-noise stimulus (peak amplitude 92 dB, C-weighting, at the egg location) via a speaker in the sound isolation chamber. The stimuli (Figure S1D) consisted of five short sound elements occurring within a 2 s period that were repeated at irregular time intervals every 12–18 s (7 repeats for the 2 min stimuli, 16 for the 5 min stimuli). Some embryos were stimulated with the chicken stimulus for the first 15 min (47 repeats). All embryos were left in silence for the last 5 min of their recording period. All except three of the embryos studied were given a lethal overdose of anesthetic so that the amount of radioactivity in their isolated heads could be measured prior to imaging; this provided a quantitative basis for interpreting intensity values on the PET images. The three exceptions were multiply imaged and treated as above after their last imaging session.

All image processing for data analysis used standard techniques, as adapted for small-animal imaging [54, 55]. Image values were normalized among embryos by referencing them to the maximum uptake value found in the pituitary gland, a structure that is connected to the brain and consistently metabolically active (further explained and validated in the Supplemental Experimental Procedures). Before analyzing behavioral differences and the effects of sound stimulation, data from four late-stage birds who had vocalized during their recording period were removed to avoid confounding analyses referring to stimulus condition. To assure comparability between the experimental conditions for chicken-stimulated and filtered-noise-stimulated birds, we also removed data from a group of embryos given chicken stimulation for 15 min. Further methodological details and

analyses are provided in the Supplemental Experimental Procedures and Supplemental Results, respectively.

Supplemental Information

Supplemental Information includes Supplemental Results, five figures, and Supplemental Experimental Procedures and can be found with this article online at doi:10.1016/j.cub.2012.03.030.

Acknowledgments

We acknowledge support from the BBVA Foundation (Chair in Biomedicine, E.B.; associated support funds, J.-J.V. and M.D.), the National Science and Engineering Research Council of Canada (298612, E.B.), the Canadian Fund for Innovation (9908, E.B.), and the Scuola Internazionale Superiore di Studi Avanzati (E.B.). We thank A. de Francisco for assistance with the experiments; C. García-Villalba for assistance with the figures; M.L. Soto-Montenegro, A. Sisniega, M. Benito, M. Abella, I. Vidal, S. Reig, J.M. Mateos, and T. Garrido for technical assistance; J. Pascau for software tools; and M.V. Green for both technical and intellectual contributions.

Received: February 14, 2012
Revised: March 13, 2012
Accepted: March 13, 2012
Published online: May 3, 2012

References

1. Siegel, J.M. (2009). The neurobiology of sleep. Semin. Neurol. *29*, 277–296.
2. Lesku, J.A., Martinez-Gonzalez, D., and Rattenborg, N.C. (2009). Phylogeny and ontogeny of sleep. In The Neuroscience of Sleep, R. Stickgold and M. Walker, eds. (Oxford: Academic Press), pp. 61–69.
3. Pace-Schott, E.F. (2009). Sleep architecture. In The Neuroscience of Sleep, R. Stickgold and M. Walker, eds. (Oxford: Academic Press), pp. 11–17.
4. Dang Vu, T.T., Desseilles, M., Peigneux, P., Laureys, S., and Maquet, P. (2009). Sleep and sleep states: PET activation patterns. In The Neuroscience of Sleep, R. Stickgold and M. Walker, eds. (Oxford: Academic Press), pp. 30–36.
5. Cirelli, C., and Tononi, G. (2011). Molecular neurobiology of sleep. In Handbook of Clinical Neurology, P.J. Vinken and G.W. Bruyn, eds. (New York: Elsevier), pp. 191–203.
6. Mendelson, W.B., James, S.P., Garnett, D., Sack, D.A., and Rosenthal, N.E. (1986). A psychophysiological study of insomnia. Psychiatry Res. *19*, 267–284.
7. Perrin, F., García-Larrea, L., Mauguière, F., and Bastuji, H. (1999). A differential brain response to the subject's own name persists during sleep. Clin. Neurophysiol. *110*, 2153–2164.
8. Portas, C.M., Krakow, K., Allen, P., Josephs, O., Armony, J.L., and Frith, C.D. (2000). Auditory processing across the sleep-wake cycle: simultaneous EEG and fMRI monitoring in humans. Neuron *28*, 991–999.
9. Prechtl, H.F.R. (1985). Ultrasound studies of human fetal behaviour. Early Hum. Dev. *12*, 91–98.
10. Mellor, D.J., and Diesch, T.J. (2007). Birth and hatching: key events in the onset of awareness in the lamb and chick. N. Z. Vet. J. *55*, 51–60.
11. Peters, J.J., Vondrahe, A.R., and Powers, T.H. (1956). The functional chronology in developing chick nervous system. J. Exp. Zool. *133*, 505–518.
12. Peters, J.J., Vondrahe, A.R., and Huesman, A.A. (1960). Chronological development of electrical activity in the optic lobes, cerebellum, and cerebrum of the chick embryo. Physiol. Zool. *33*, 225–231.
13. Peters, J.J., Vonderahe, A., and Schmid, D. (1965). Onset of cerebral electrical activity associated with behavioral sleep and attention in the developing chick. J. Exp. Zool. *160*, 255–261.
14. Corner, M.A., Bakhuis, W.L., and van Wingerden, C. (1973). Sleep and wakefulness during early life in the domestic chicken, and their relationship to hatching and embryonic motility. In Studies on the Development of Behavior and the Nervous System, Volume 1: Behavioral Embryology, G. Gottlieb, ed. (New York: Academic Press), pp. 245–279.
15. Rigatto, H., Moore, M., and Cates, D. (1986). Fetal breathing and behavior measured through a double-wall Plexiglas window in sheep. J. Appl. Physiol. *61*, 160–164.
16. Karlsson, K.Æ., Arnardóttir, H., Robinson, S.R., and Blumberg, M.S. (2011). Dynamics of sleep-wake cyclicity across the fetal period in sheep (Ovis aries). Dev. Psychobiol. *53*, 89–95.
17. Ruckebusch, Y. (1972). Development of sleep and wakefulness in the foetal lamb. Electroencephalogr. Clin. Neurophysiol. *32*, 119–128.
18. Szeto, H.H., and Hinman, D.J. (1985). Prenatal development of sleep-wake patterns in sheep. Sleep *8*, 347–355.
19. Corner, M.A., Schadé, J.P., Sedláček, J., Stoeckart, R., and Bot, A.P.C. (1967). Developmental patterns in the central nervous system of birds. I. Electrical activity in the cerebral hemisphere, optic lobe and cerebellum. Prog. Brain Res. *26*, 145–192.
20. Woods, J.R., Jr., Plessinger, M.A., and Mack, C.E. (1984). Fetal auditory brainstem evoked response (ABR). Pediatr. Res. *18*, 83–85.
21. Cook, C.J., Williams, C., and Gluckman, P.D. (1987). Brainstem auditory evoked potentials in the fetal sheep, in utero. J. Dev. Physiol. *9*, 429–439.
22. Cook, C.J., Gluckman, P.D., Johnston, B.M., and Williams, C. (1987). The development of the somatosensory evoked potential in the unanaesthetized fetal sheep. J. Dev. Physiol. *9*, 441–455.
23. Corner, M.A., and Bot, A.P.C. (1967). Developmental patterns in the central nervous system of birds. 3. Somatic motility during the embryonic period and its relation to behavior after hatching. Prog. Brain Res. *26*, 214–236.
24. Corner, M.A., and Bakhuis, W.L. (1969). Developmental patterns in the central nervous system of birds. V. Cerebral electrical activity, forebrain function and behavior in the chick at the time of hatching. Brain Res. *13*, 541–555.
25. Sedláček, J. (1976). Acoustic and somatosensory evoked responses in the brain hemispheres of chick embryos. Physiol. Bohemoslov. *25*, 103–108.
26. Jackson, H., and Rubel, E.W. (1978). Ontogeny of behavioral responsiveness to sound in the chick embryo as indicated by electrical recordings of motility. J. Comp. Physiol. Psychol. *92*, 682–696.
27. Abrams, R.M., Schwab, M., Gerhardt, K.J., Bauer, R., and Peters, A.J.M. (1996). Vibroacoustic stimulation with a complex signal: effect on behavioral state in fetal sheep. Biol. Neonate *70*, 155–164.
28. Bauer, R., Schwab, M., Abrams, R.M., Stein, J., and Gerhardt, K.J. (1997). Electrocortical and heart rate response during vibroacoustic stimulation in fetal sheep. Am. J. Obstet. Gynecol. *177*, 66–71.
29. Schwab, M., Schmidt, K., Witte, H., and Abrams, M. (2000). Investigation of nonlinear ECoG changes during spontaneous sleep state changes and cortical arousal in fetal sheep. Cereb. Cortex *10*, 142–148.
30. Wang, Y., Seidel, J., Tsui, B.M.W., Vaquero, J.J., and Pomper, M.G. (2006). Performance evaluation of the GE healthcare eXplore VISTA dual-ring small-animal PET scanner. J. Nucl. Med. *47*, 1891–1900.
31. Vaquero, J.J., Redondo, S., Lage, E., Abella, M., Sisniega, A., Tapias, G., Soto-Montenegro, M.L., and Desco, M. (2008). Assessment of a new high-performance small-animal X-ray tomograph. IEEE Trans. Nucl. Sci. *55*, 898–905.
32. Hamilton, H.L., and Hamburger, V. (1951). A series of normal stages in the development of the chick embryo. J. Morphol. *88*, 49–92.
33. Kovach, J.K., Callies, D., and Hartzell, R. (1970). Procedures for the study of behavior in avian embryos. Dev. Psychobiol. *3*, 169–178.
34. Park, T., and Balaban, E. (1991). Relative salience of species maternal calls in neonatal gallinaceous birds: A direct comparison of Japanese quail (Coturnix coturnix japonica) and domestic chickens (Gallus gallus domesticus). J. Comp. Psychol. *105*, 45–54.
35. Long, K.D., Kennedy, G., and Balaban, E. (2001). Transferring an inborn auditory perceptual predisposition with interspecies brain transplants. Proc. Natl. Acad. Sci. USA *98*, 5862–5867.
36. Luppi, P.H., Gervasoni, D., Verret, L., Goutagny, R., Peyron, C., Salvert, D., Leger, L., and Fort, P. (2006). Paradoxical (REM) sleep genesis: The switch from an aminergic-cholinergic to a GABAergic-glutamatergic hypothesis. J. Physiol. Paris *100*, 271–283.
37. Fuller, P.M., Sherman, D., Pedersen, N.P., Saper, C.B., and Lu, J. (2011). Reassessment of the structural basis of the ascending arousal system. J. Comp. Neurol. *519*, 933–956.
38. Lo, C.C., Chou, T., Penzel, T., Scammell, T.E., Strecker, R.E., Stanley, H.E., and Ivanov, P.Ch. (2004). Common scale-invariant patterns of sleep-wake transitions across mammalian species. Proc. Natl. Acad. Sci. USA *101*, 17545–17548.
39. Blumberg, M.S., Seelke, A.M., Lowen, S.B., and Karlsson, K.Æ. (2005). Dynamics of sleep-wake cyclicity in developing rats. Proc. Natl. Acad. Sci. USA *102*, 14860–14864.

40. Blumberg, M.S., Coleman, C.M., Johnson, E.D., and Shaw, C. (2007). Developmental divergence of sleep-wake patterns in orexin knockout and wild-type mice. Eur. J. Neurosci. *25*, 512–518.
41. Ben-Ari, Y., Gaiarsa, J.L., Tyzio, R., and Khazipov, R. (2007). GABA: a pioneer transmitter that excites immature neurons and generates primitive oscillations. Physiol. Rev. *87*, 1215–1284.
42. Fiumelli, H., and Woodin, M.A. (2007). Role of activity-dependent regulation of neuronal chloride homeostasis in development. Curr. Opin. Neurobiol. *17*, 81–86.
43. O'Donovan, M.J. (1999). The origin of spontaneous activity in developing networks of the vertebrate nervous system. Curr. Opin. Neurobiol. *9*, 94–104.
44. Hanson, M.G., and Landmesser, L.T. (2004). Normal patterns of spontaneous activity are required for correct motor axon guidance and the expression of specific guidance molecules. Neuron *43*, 687–701.
45. Gonzalez-Islas, C., and Wenner, P. (2006). Spontaneous network activity in the embryonic spinal cord regulates AMPAergic and GABAergic synaptic strength. Neuron *49*, 563–575.
46. Liu, Z., Neff, R.A., and Berg, D.K. (2006). Sequential interplay of nicotinic and GABAergic signaling guides neuronal development. Science *314*, 1610–1613.
47. Xu, H., Whelan, P.J., and Wenner, P. (2005). Development of an inhibitory interneuronal circuit in the embryonic spinal cord. J. Neurophysiol. *93*, 2922–2933.
48. Ring, H., Boije, H., Daniel, C., Ohlson, J., Öhman, M., and Hallböök, F. (2010). Increased A-to-I RNA editing of the transcript for $GABA_A$ receptor subunit $\alpha 3$ during chick retinal development. Vis. Neurosci. *27*, 149–157.
49. Blumberg, M.S., Karlsson, K.Æ., Seelke, A.M.H., and Mohns, E.J. (2005). The ontogeny of mammalian sleep: a response to Frank and Heller (2003). J. Sleep Res. *14*, 91–98.
50. Karlsson, K.Æ., Gall, A.J., Mohns, E.J., Seelke, A.M.H., and Blumberg, M.S. (2005). The neural substrates of infant sleep in rats. PLoS Biol. *3*, e143.
51. Frank, M.G., and Heller, H.C. (2003). The ontogeny of mammalian sleep: a reappraisal of alternative hypotheses. J. Sleep Res. *12*, 25–34.
52. Frank, M.G., and Heller, H.C. (2005). Unresolved issues in sleep ontogeny: a response to Blumberg et al. J. Sleep Res. *14*, 98–101.
53. de Villers-Sidani, E., and Merzenich, M.M. (2011). Lifelong plasticity in the rat auditory cortex: basic mechanisms and role of sensory experience. Prog. Brain Res. *191*, 119–131.
54. Pascau, J., Vaquero, J.J., Abella, M., Cacho, R., Lage, E., and Desco, M. (2006). Multimodality workstation for small animal image visualization and analysis. Mol. Imaging Biol. *8*, 97–98.
55. Pascau, J., Gispert, J.D., Michaelides, M., Thanos, P.K., Volkow, N.D., Vaquero, J.J., Soto-Montenegro, M.L., and Desco, M. (2009). Automated method for small-animal PET image registration with intrinsic validation. Mol. Imaging Biol. *11*, 107–113.

Current Biology, Volume *22*

Supplemental Information

Waking-like Brain Function in Embryos

Evan Balaban, Manuel Desco, and Juan-José Vaquero

Author Contributions

E.B. and J.-J.V. conceived the study; E.B., M.D., and J.-J.V. designed the experiments; E.B. and J.-J.V. carried out the experiments; E.B. analyzed the data; and E.B. and J.-J.V. wrote the paper.

Supplemental Inventory

Supplemental Results

Additional Analyses of Embryo Brain Metabolic Patterns

Figure S2A shows the correlation between the maximum activity value in the telencephalon and the maximum activity value in cerebellum in individual birds ($r = 0.96$, $n = 201$, $p < 0.0001$). The correlation coefficients for embryos in the three sound stimulus conditions were identical to each other (Silence: $r = 0.96$, $n = 51$, $p < 0.001$; Filtered Noise: $r = 0.96$, $n = 51$, $p < 0.001$, Chicken Sound: $r = 0.96$, $n = 95$, $p < 0.001$).

Figure S2B shows the locations of metabolic activity within 15% of the higher-brain maximum, shared by at least 50% of the embryos within each brain pattern / developmental stage category, and transformed to a standard spatial template for each developmental stage. Activated areas included: [bilateral forebrain] hyperpallium / mesopallium; [cerebellum] a single region including the bilateral deep cerebellar nuclei; [ventral brainstem] rPRF (present in fActive embryos, but generally below 15% of the maximum value in the higher brain). The brain regions with the greatest activity were similar across all metabolic categories and developmental stages.

We conducted statistical analyses to see if there were any fluctuations in the proportion of different brain metabolic patterns with time of day (our experiments were conducted between 8:00-21:00); there were no significant differences in proportions among different time periods when the experimental times in this interval were divided into hourly periods, or into 3 periods – before 12:00, from 12:00-17:00, after 17:00 (all $p > 0.25$). Since the eggs were incubated in darkness, even if individual embryos had circadian variation in brain activation, the patterns would not necessarily be entrained among different embryos, and so would not show up as a population-level fluctuation.

Additional Analyses of Sound Stimulation Effects on Brain and Behavior

We divided the brain metabolic activation data by sound stimulus (chicken (C) and filtered noise (FN)) and developmental stage (Age II or Age IV) to examine the effects of stimulus duration. For the C-stimulation condition, there were no significant differences in the frequency of rActive embryos between 5-min and 15-min presentations (Age II: 43% for 5-min vs. 50% for 15-min; Age IV: both 89%), so we combined the data for these two presentation lengths within each developmental stage. There were no significant differences in the proportion of rActive brains produced by sound presentations of 2-min durations vs. the longer durations at either developmental stage for the filtered-noise or chicken stimuli (FN: Age II, $G = 0.03$, $p = 0.87$; Age IV, $G = 0.16$, $p = 0.69$; C: Age II, $G = 0.63$, $p = 0.43$; Age IV, $G = 2.83$, $p = 0.09$).

We did not find any reliable movement or heart-rate response differences temporally locked to stimulus presentation (that is, occurring within a 30-second period after the beginning of each sound stimulus, all $p > 0.20$). However, dynamic changes in the number and average duration of movement bouts did show differences when comparing the period 5 minutes before stimulation began (measured at an equivalent time in embryos exposed to silence) with the 5 minute period after stimulation began (Figure S3A). Here, rInactive embryos showed significantly different changes in both number and mean duration of movement bouts in sound-stimulated as compared to silent conditions (with sound-stimulated embryos showing relatively larger changes in both). This relationship held for the developmental periods prior to Age IV

(Mann-Whitney Tests, Sound (n = 42) vs. Silence (n = 11), movement number ratio: p = 0.004, movement duration ratio: p = 0.03), when rInactive embryos do not have quiescent period durations distributed like sleep, but not at Age IV (Sound (n = 15) vs. Silence (n = 10), movement number ratio: p = 0.78, movement duration ratio: p = 0.44). There were no stimulus-based differences in movement responses for pActive embryos, and fActive embryos showed significant differences in the ratio of both the number and mean duration of movements among all three stimulation conditions (with chicken-stimulated embryos having the largest changes in both).

Since rInactive embryos at Ages II/III and IV exhibited changes in behavior in response to sound stimulation, in the absence of major changes in the magnitude of glucose uptake in higher brain regions, we wondered if stimulation led to more subtle changes in the distribution of their brain glucose uptake patterns. Although there were no stimulus-related differences in the mean (first moment) or the variance (second moment) of the brain distributions (not shown), there were significant increases in skewness ("asymmetry", third moment, Kruskal-Wallis test, H = 14.54, df = 3, p = 0.0023) and kurtosis ("peakedness", fourth moment, Kruskal-Wallis test, H = 74.50, df = 3, p < 0.0001) [Figure S3B]. The biological interpretation of these changes is as follows. Brain metabolic activity values were distributed over a narrow range in rInactive embryos; sound stimulation caused a reliable shift of these values away from the center (around the "peak" of the distribution) and into the "tails" (producing the significant positive increase in kurtosis in the population of sound-stimulated rInactive embryos). There were reliably more relative increases in metabolic activation than decreases, so the "upper tails" of the brain distributions became longer than the "lower tails" (producing the significant positive increase in skewness). The means did not change significantly because the overall effects of these positive and negative shifts partially cancelled each other; the variance did not significantly increase because the changes in value were not extreme enough. Posthoc tests corrected for multiple comparisons ($p < 0.05$) showed that significant changes to sound stimulation occurred in these parameters for rInactive but not rActive brains (Figure S3B).

Significant differences also occurred in the spatial extent of activation in the cerebellar and telencephalic regions identified in Figure S2B. In the cerebellum, the volume of activation at 85% of the maximum value was significantly smaller in sound-stimulated rInactive embryos than in silent ones (Kruskal-Wallis test, H = 9.45, df = 2, p = 0.009; posthoc tests corrected for multiple comparisons, $p < 0.05$, Figure S3C, left), while the telencephalic volume of activation was smaller in filtered-noise-stimulated rInactive embryos than in the two other groups (Kruskal-Wallis test, H = 7.34, df = 2, p = 0.026; posthoc tests corrected for multiple comparisons, $p < 0.05$, Figure S3C, right).

The developmentally least-advanced (Age 1) rInactive embryos also showed behavioral and brain response differences to stimulation. Embryos exposed to the filtered-noise stimulus showed greater values of normalized movement duration change (the average movement duration during the 5 minutes after stimulation minus the average during the five minutes before stimulation, divided by the overall mean movement duration; mean$\pm$ sd: S (n = 5), -2.4 $\pm$ 5.5 %; FN (n = 10), 19.0 $\pm$ 5.4 %; C (n = 9), -5.1 $\pm$ 6.7 %; Kruskal-Wallis test: H = 6.36, df = 2, p = 0.042). Filtered-noise-stimulated embryos were also the only ones with change values significantly greater than zero (Wilcoxon tests corrected for 3 comparisons, $p > 0.95$ for S,C stimuli, p = .038 for FN). This behavioral variable also had significantly different correlations

with the telencephalic volume of activation for filtered-noise- and chicken-sound-stimulated Age 1 embryos (FN: r = -0.71, n = 10, p = 0.019; C: r = 0.52, n = 9, p = 0.16; S: r = -0.13, n = 5, p = 0.86; χ^2 for heterogeneity = 6.88, df = 2, p < 0.032; multiply-corrected FN-C comparison, p< 0.026, C-S and FN-S comparisons both p > 0.95). This demonstrated that the lack of rActive brain responses observed at Age I was not due to either a lack of transmission of external sensory information to the brain, or a lack of responsiveness of the brain to sensory stimulation.

Additional Analyses of Stimulus-Exclusive Induction of Correlated Activity between Brain Areas

Approximately 33 % (15-min-stimulated embryos excluded) - 40 % (15-min-stimulated embryos included) of all chicken-stimulated fActive embryos had elevated rPRF levels and MRF/rPRF ratios (respective p-values are 0.042 and 0.0009, df = 1, relative to 0 % for non-chicken-stimulated fActive embryos, Fisher's exact test). Excluding embryos stimulated for 15-minutes, chicken- and filtered-noise-stimulated fActive embryos also had significantly different, oppositely-signed correlations between rPRF glucose uptake and MRF/rPRF ratios (C: r = 0.79, n = 15; FN: r = -0.34, n = 7; difference, p = 0.008). The group of chicken-stimulated fActive embryos with elevated rPRF maxima and MRF/rPRF ratios also had significantly higher glucose uptake levels in the telencephalon and cerebellum (Kruskal-Wallis test, H = 14.05, df = 2, p = 0.009, 15-min birds included; H = 9.20, df = 2, p = 0.01, 15-min birds excluded, Figure S4A), and a larger increase in the number of movement bouts after stimulation than other fActive embryos (H = 6.81, df = 2, p = 0.03 Figure S4B); all chicken-stimulated fActive embryos also had greater post-stimulation changes in movement bout length than their counterparts (H = 8.43, df = 2, p = 0.015, Figure S4C).

Figure S5 shows the correlation between rPRF maxima and telencephalon / cerebellum maxima divided according to developmental stage. The probabilities were corrected for 12 comparisons [2 developmental stages (Ages II/III, and IV) x 2 brain patterns (rInactive, rActive) x 3 stimulus conditions (S [silent], FN [filtered noise], C [chicken])]; none of the S or FN correlations were significant. The correlation is significantly positive for rInactive and (marginally) for rActive embryos at Age II / III, and for rActive embryos only at Age IV. Therefore, chicken-stimulation resulted in a correlation between metabolic activity in the brainstem and higher brain at all developmental stages where stimulation affected the magnitude of higher-brain glucose metabolic responses, except in the condition that showed the highest resemblance to NREM sleep (rInactive Age IV embryos).

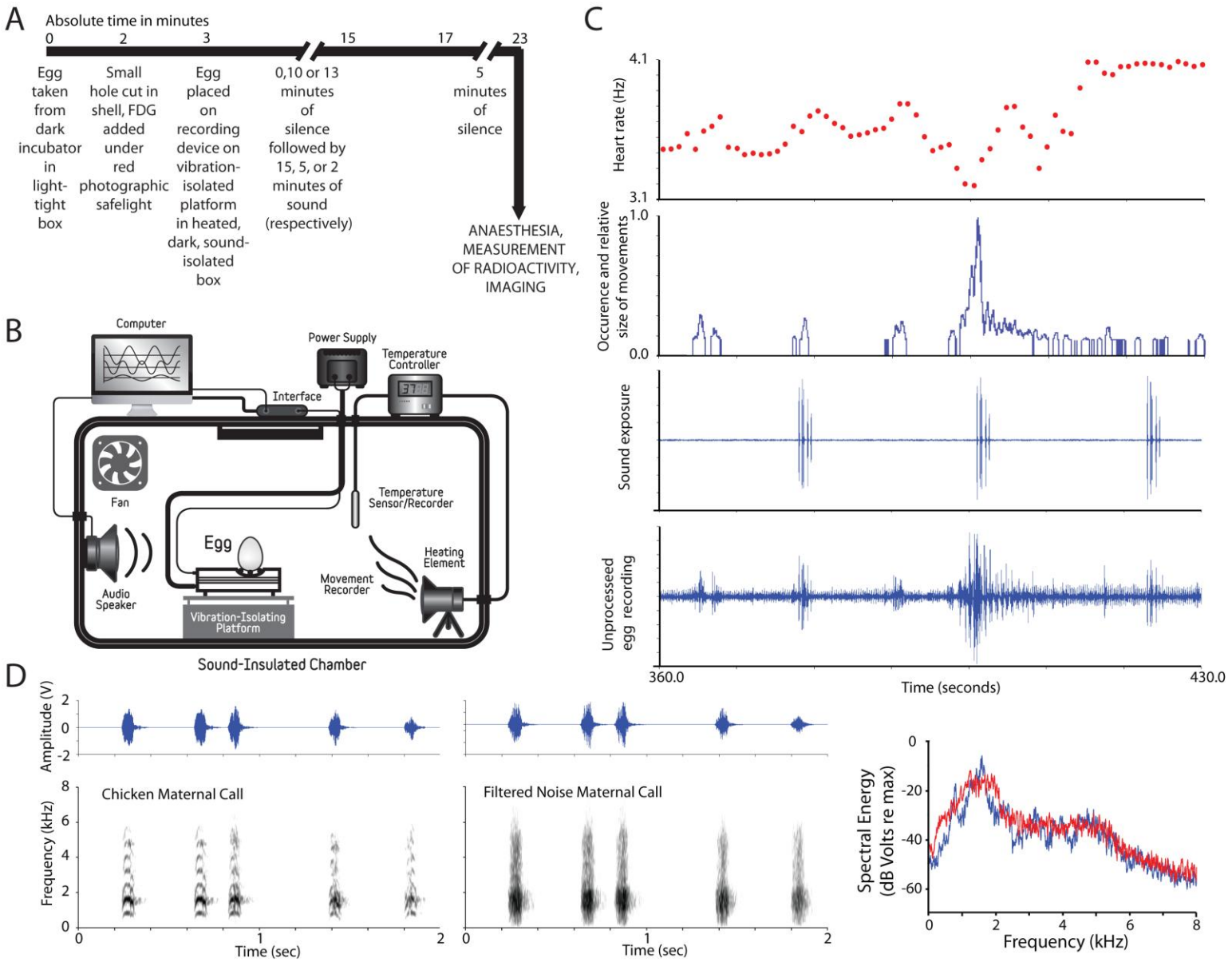
A
Absolute time in minutes
0
2
3
15
17
23
Egg taken from dark incubator in light-tight box
Small hole cut in shell, FDG added under red photographic safelight
Egg placed on recording device on vibration-isolated platform in heated, dark, sound-isolated box
0,10 or 13 minutes of silence followed by 15, 5, or 2 minutes of sound (respectively)
5 minutes of silence
ANAESTHESIA, MEASUREMENT OF RADIOACTIVITY, IMAGING
B
Computer
Power Supply
Temperature Controller
Interface
Fan
Temperature Sensor/Recorder
Egg
Heating Element
Movement Recorder
Audio Speaker
Vibration-Isolating Platform
Sound-Insulated Chamber
C
Heart rate (Hz)
4.1
3.1
Occurence and relative size of movements
1.0
0.0
Sound exposure
Unprocesseed egg recording
360.0
430.0
Time (seconds)
D
Amplitude (V)
Chicken Maternal Call
Filtered Noise Maternal Call
Frequency (kHz)
Time (sec)
Spectral Energy (dB Volts re max)
Frequency (kHz)

Figure S1.

Figure S1. Experimental Details and Sample Data

(A) The time line for the imaging experiments.

(B) Diagram of the experimental setup.

(C) Example of behavioral data recorded from eggs. (Bottom) Raw amplitude [y-axis, arbitrary units] – time (seconds) waveform from a sound-exposed embryo (stimulus amplitude-time waveform, 2nd from bottom), together with the movement-time waveform derived by signal-processing from the raw recording (2nd from top, y-axis units : Volts), and the heart-rate contour also derived by signal processing (top, y-axis units: Hertz).

(D) Sound stimuli used in the experiments (left and middle, amplitude-time (top) and wide-band spectrographic representations (bottom); right, spectral energy [y-axis] versus frequency [x-axis] plot; the chicken stimulus is in blue, the filtered noise stimulus is in red.

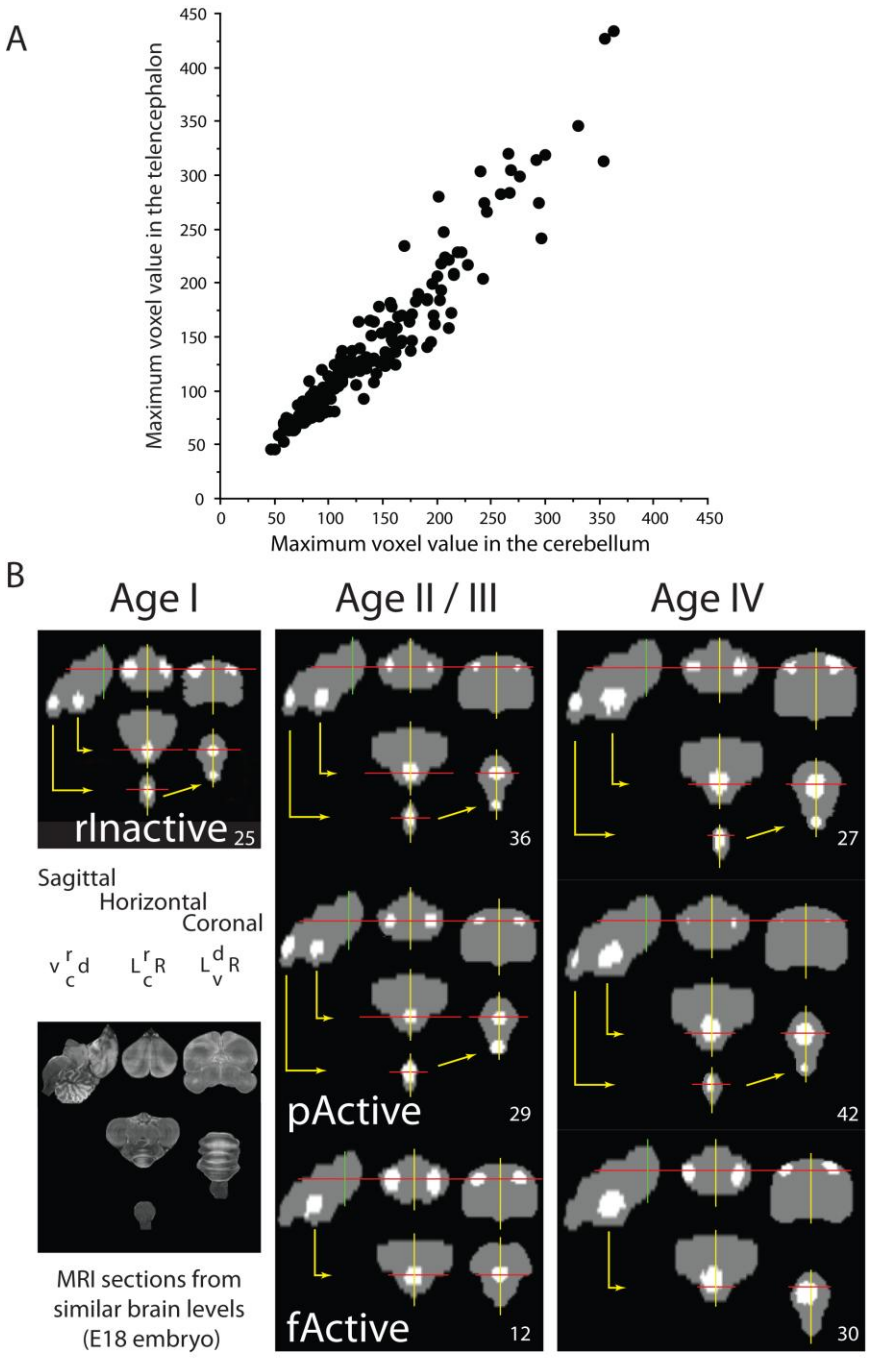

Figure S2. Additional Analyses of Embryo Brain Activation Patterns

(A) Maximum voxel values in the telencephalon (y-axis) and cerebellum (x-axis) for all 201 embryos.

(B) The locations of metabolic activity within 15% of the higher-brain maximum, shared by at least 50% of the embryos within each brain pattern / developmental stage category. Each gray area represents a 2-dimensional projection of the brain from a sagittal, horizontal, or coronal perspective (r = rostral, c = caudal, L = left, R = right, d = dorsal, v = ventral); structural MRI images from similar levels of the brain are shown at the lower left. Numbers are sample sizes.

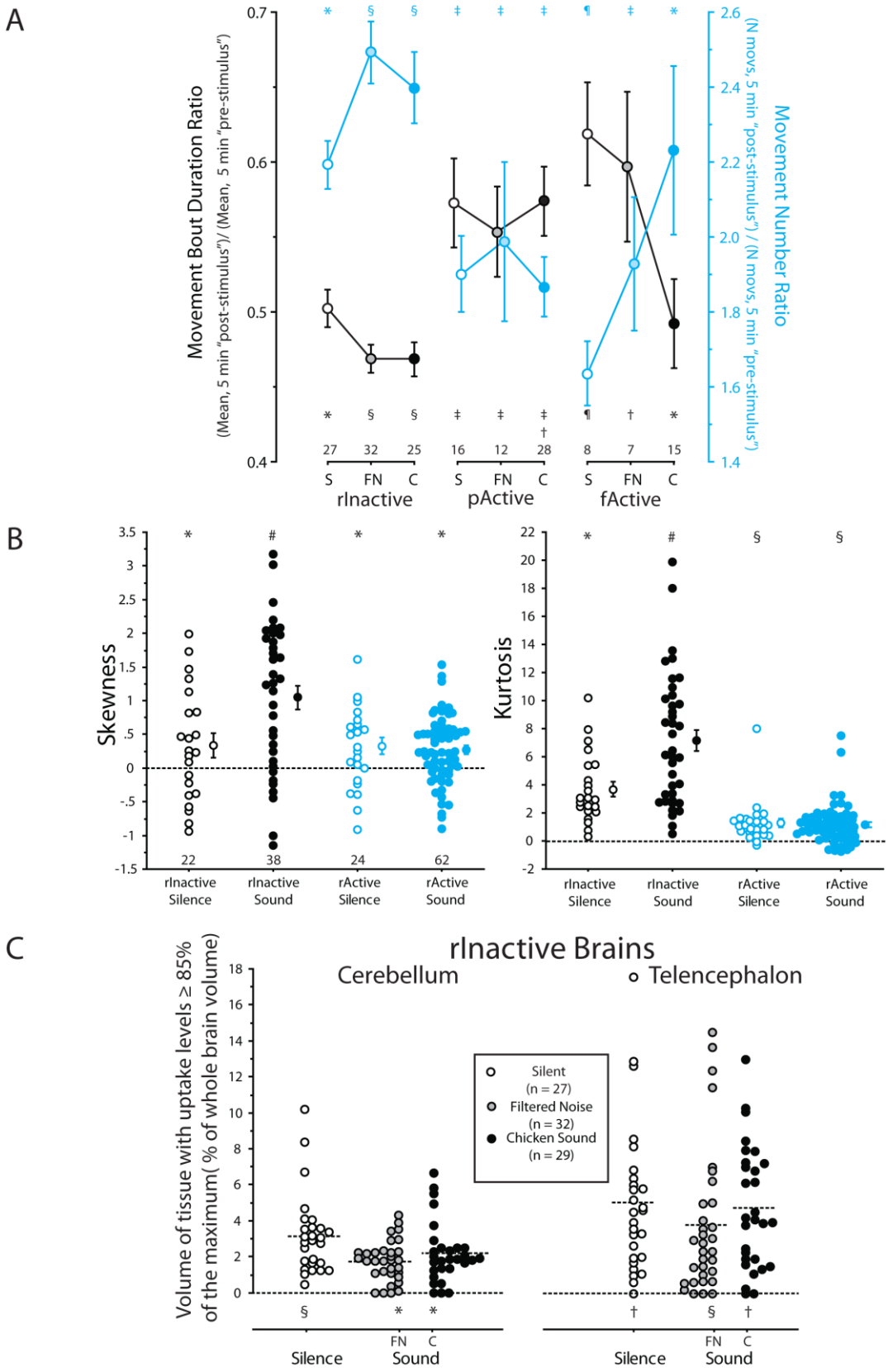
A
Movement Bout Duration Ratio
(Mean, 5 min "post-stimulus")/ (Mean, 5 min "pre-stimulus")
Movement Number Ratio
(N movs, 5 min "post-stimulus") / (N movs, 5 min "pre-stimulus")
0.7
0.6
0.5
0.4
2.6
2.4
2.2
2.0
1.8
1.6
1.4
27 32 25
16 12 28
8 7 15
S FN C
rInactive
pActive
fActive
B
Skewness
Kurtosis
3.5
3
2.5
2
1.5
1
.5
0
-.5
-1
-1.5
22
38
24
62
rInactive Silence
rInactive Sound
rActive Silence
rActive Sound
C
rInactive Brains
Cerebellum
Telencephalon
Volume of tissue with uptake levels ≥ 85% of the maximum(% of whole brain volume)
Silent (n = 27)
Filtered Noise (n = 32)
Chicken Sound (n = 29)
Silence
Sound
FN
C

Figure S3.

Figure S3. Additional Analyses of Sound Stimulation Effects on Brain and Behaviour

(A) Movement bout duration ratios (black) and movement number ratios (blue) [y-axis], plotted by brain pattern and stimulus condition [x-axis]. Movement bout duration ratios = mean movement bout duration during the 5 minutes after the stimulus began (or the equivalent time in silence-exposed embryos), divided by the mean movement bout duration 5 minutes before the stimulus began; movement number ratios = the number of movement bouts during the 5 minutes after the stimulus began (or the equivalent time in silence-exposed embryos), divided by the number of movement bouts before the stimulus began. Symbols at the top and bottom of the graph represent the results of post-hoc tests corrected for multiple comparisons based on a Kruskal-Wallis ANOVA (Movement bout duration ratio: df = 8, H = 35.99, $p < 0.0001$; movement number ratio H = 45.22, df = 8, $p < 0.0001$); points with different symbols are significantly different from each other ($p < 0.05$ level). Sample sizes are given below each point. Error bars are $\pm$ 1 sem.

(B) Skewness (third moment, left) and kurtosis (fourth moment, right) of the whole-brain distribution of glucose uptake values [y-axis] by brain pattern and stimulus condition [Sound or Silence, x-axis]. The filtered noise and chicken conditions were combined because they exhibited similar distributions. The dots with error bars ($\pm$ 1 sem) are means of the scatterplots to the left of them. Symbols at the top of the graph represent the results of post-hoc tests corrected for multiple comparisons ($p < 0.05$). Sample sizes are given at the bottom of the graph.

(C) Volume (% of whole brain volume) of brain tissue with glucose uptake levels $\geq$ 85% of the maximum value above the rPRF [y-axis] versus sound exposure condition [x-axis] for the cerebellum (left) and telencephalon (right). Dotted lines indicate the mean values of each group. Symbols at the bottom of the graph represent the results of post-hoc tests corrected for multiple comparisons ($p < 0.05$).

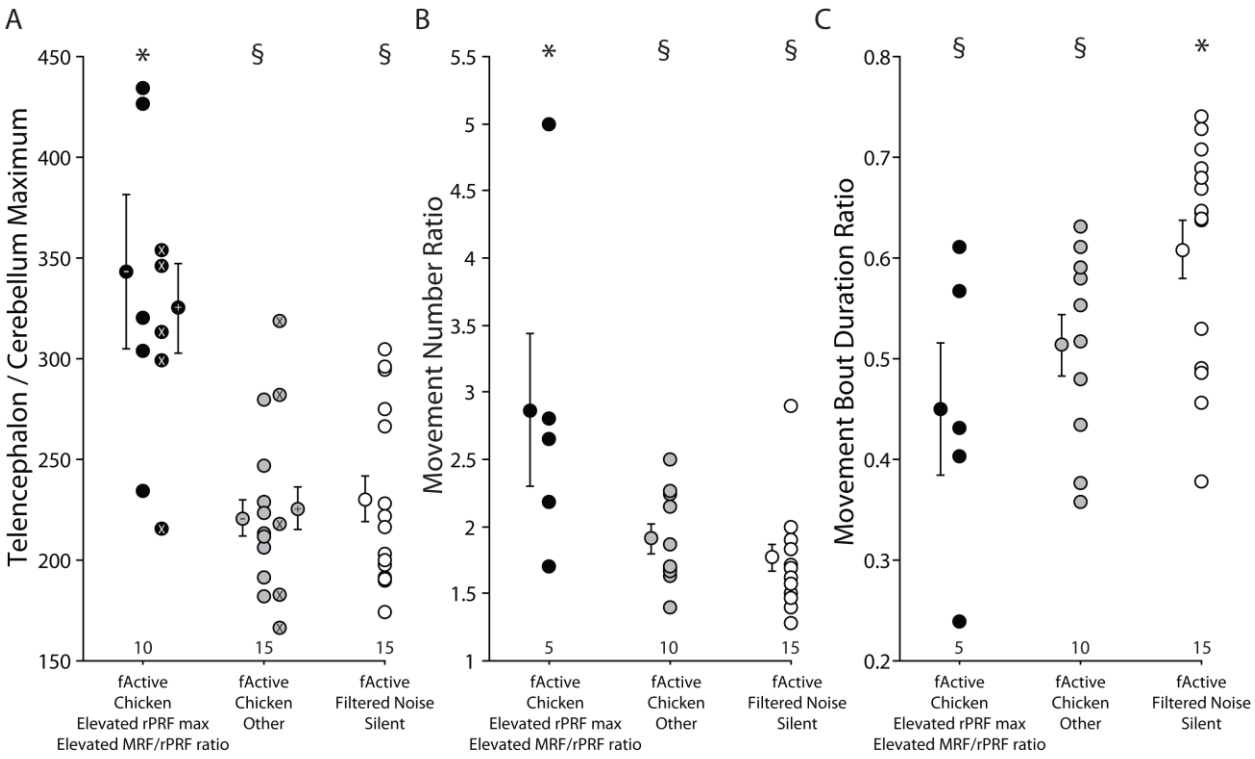

Figure S4. **Additional Analyses of the Effects of Sound Stimulation on fActive Embryo Brain Activation and Behaviour**

(A) The maximum glucose uptake value in the telencephalon or cerebellum (whichever was higher) [y-axis] plotted against three categories of fActive embryos: (leftmost) chicken-stimulated with elevated rPRF and MRF/rPRF ratio values (see Figure 6A), (center) all other fActive chicken stimulated embryos, (rightmost) fActive embryos exposed to filtered-noise or silence. An "x" indicates a data point from an embryo given 15-minute chicken stimulation. Points with error bars ($\pm$ 1 sem) indicate means; "+" includes 15-min birds, "-" excludes them. Symbols at the top of the graph represent the results of post-hoc tests corrected for multiple comparisons ($p < 0.05$; significance indications are the same for tests including or excluding embryos stimulated for 15-min). Sample sizes are given at the bottom of the graph.

(B and C) Movement number ratio (B) and movement bout duration ratio (C) (see Figure S3A) for the same groups shown in (A); error bars, significance designations, and sample sizes are given as above.

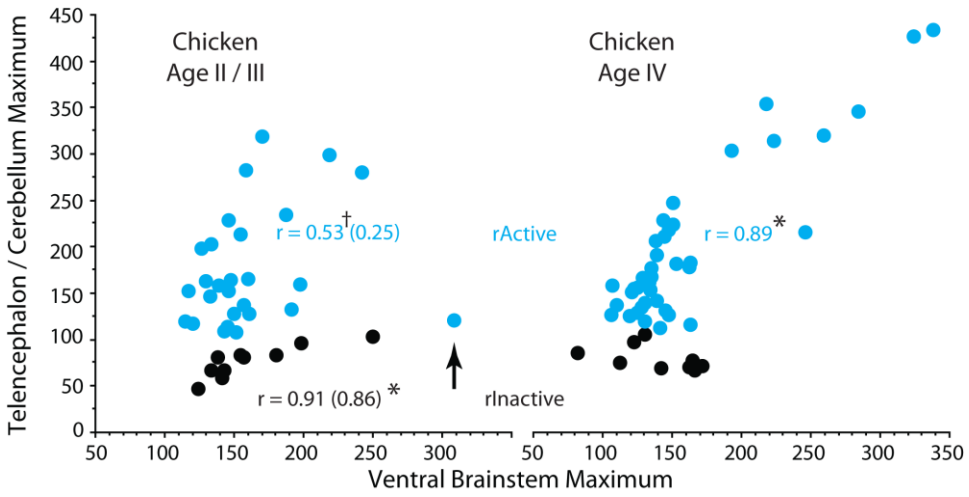

Figure S5. Additional Analyses of the Activity Correlation between Brain Regions

The correlation between maximum values in the telencephalon / cerebellum (whichever had the higher value,[y-axis]) and the ventral brainstem [x-axis]. Data from chicken-stimulated embryos is divided according to developmental stage and brain pattern. The arrow indicates an outlying embryo that was classified as rActive based on its maximal glucose level above the ventral brainstem (Figure 1B), but, based on the other data at its developmental stage, it appears to better fit with the "constrained" glucose uptake levels of rInactive embryos. The correlation values in parentheses are based on counting it as rActive; correlation values outside of parentheses are based on counting it as rInactive. All p-values were corrected for 12 implicit multiple comparisons [2 developmental stages (Ages II/III, and IV) x 2 brain patterns (rInactve, rActive) x 3 stimulus conditions (silence, filtered noise, chicken)]. Only significant values (*) or marginally significant values (†, p = 0.052) are shown.

Supplemental Experimental Procedures

The Choice of Imaging Modality

The primary purpose of this study was to collect information on brain metabolic activity in embryos using the least invasive conditions possible. PET/CT imaging was chosen because it allowed subjects to continue their normal behavior without any constraints while tracer molecules were being taken up by their brain, muscle and organ systems, and because it avoided sensory stimulation confounds due to the noise and vibration associated with functional or structural magnetic resonance imaging. The requirement for minimally- invasive conditions limited us to studying the temporally-integrated uptake of tracer over the entire 20-minute experimental period. This is why behavioral analyses were conducted with reference to relative durations or proportions of events over the whole experimental period. The results obtained here will serve as a reference point for future studies incorporating more invasive manipulations.

Subjects, Their Preparation for Imaging, and Sound Stimuli

All animal use in these experiments was reviewed and approved by the local animal use committee. Data from 223 birds were used for this study. Sixteen of these were 1-2 day-old posthatching birds obtained from a commercial hatchery; the other 207 were obtained as fertilized eggs from commercial sources and incubated as described below. Nine of these 207 embryos were imaged multiple times; the other 198 were imaged only once. The major dataset consisted of 201 embryos, 198 imaged once at various ages, together with the final imaging sessions of 3 multiply-imaged embryos. A diagram of the experimental time-course is shown in Figure S1A.

Of the 201 embryos analyzed here, 51 were imaged after no exposure to sound stimulation (silent condition), 51 after exposure to the filtered-noise stimulus (filtered noise condition, 37 for two minutes, 14 for 5 minutes), and 91 after exposure to the chicken stimulus (chicken condition, 44 for 2 minutes, 24 for 5 minutes, 27 for fifteen minutes). The stimuli used in these experiments are shown in Figure S1D. The chicken stimulus and its post-hatching behavioral validation have been described previously (34, 35). The filtered-noise stimulus was created using the SIGNAL digital sound-analysis system (Engineering Design, Berkeley, CA). The chicken stimulus was converted to the frequency domain, its discrete Fourier transform spectrum was smoothed with a 1 Hz window to create a spectral envelope, this was multiplied by the spectrum of uniform random (white) noise, inverse-transformed to convert it back to the time domain, and adjusted to have the same root-mean-squared (rms) amplitude as the chicken stimulus.

Egg Preparation for Imaging

Fertilized chicken eggs were incubated for 15-21 days (Hamburger-Hamilton stages 39-45 (32)) in a light-tight incubator (Brinsea Octagon 100, Somerset, UK) at 37.5° C, 55 % humidity and removed singly in a light-tight, padded container for behavioral recording and imaging.

A noninvasive method for introduction of tracer molecules was used in order to preserve the integrity of both the fibrous protective inner shell membrane, and the heavily-vascularized chorioallantoic membrane across which gas exchange takes place. 2-deoxy-2-

^{18}Fluoro-D-glucose was obtained in sterile saline solution from commercial sources, and approximately 1.5 mCi was mixed with a sufficient volume of dimethyl sulfoxide (DMSO, Sigma-Aldrich) to make the final solution 10% DMSO by volume. This was placed in a 1.0 cc syringe in a 37.5° C water bath several minutes prior to use. Under a red photographic safelight, a small (4-5 mm diameter) hole was gently cut in the shell overlying the airspace at the blunt end of the egg, and the tracer solution was applied through the hole by depositing it gently on top of the inner shell membrane in the region underlying the hole. A piece of sterile, porous wound-closure tape (3M Steri-strip Elastic Skin Closure, St. Paul, MN, USA) was used to seal up the hole, and the egg was placed on a custom-made movement-recording device (see below) atop a vibration-isolation platform (Minus-K BM-10, Inglewood, CA) inside a light-tight 37.5° C sound-isolated chamber for the 20-minute recording period prior to imaging.

DMSO has been routinely used as a low-toxicity cryoprotective solvent for biological materials, as well as a vehicle for transdermal delivery of human medicines, and has also been reported to suppress glutamate-induced neurotoxicity (56) and oxidative neuronal damage (57) in adult brains. More recently, it was found to be cytotoxic to cultured auditory hair cells prepared from postnatal day 2-3 rat pups after 24 hours of continuous exposure (58), and to affect the neurite outgrowth (but not the survival) of cultured cerebellar cells from 7-day old rat pups (59). A recent study found that intraperitoneal injections of DMSO into young postnatal C57Bl/6 mice at concentrations as low as 0.3 ml/kg increased the proportion of apoptotic cells subsequently found in their brains (60), first detectable at 2 hours after administration. Since DMSO does not appear to affect the survival of cultured neurons, it is unclear if this result reflects a developmentally-vulnerable period for increased brain cell death, or a decrease in the function of microglial cells and macrophages that scavenge dying cells, resulting in the persistence of cells with apoptotic morphology for longer periods of time. We used doses equivalent to ~0.4-0.8 ml/kg, topically applied on a fibrous “external” membrane, rather than injected directly into the body cavity. The 20 minute period between application and imaging, together with the fact that all embryos received equivalent DMSO exposure, indicates that differences in apoptosis are unlikely to explain the differences in brain glucose responses analyzed here. For multiply-imaged embryos (9 total, of which only 3 were used in the main data set), brain glucose uptake responses did not appear to be different than in singly-imaged embryos (Figure 1C).

At the end of the recording period, singly-imaged birds were removed from the sound-isolation chamber under a red photographic safelight, and immediately placed in a light-tight container containing an overdose of volatile isoflurane anesthetic (Baxter Healthcare, Deerfield, IL) for 2 minutes. The egg was then quickly opened, and the embryo head was removed at or below the 6th cervical vertebra with a surgical scissors, and rinsed several times with warm saline. It was next placed in a 25-ml plastic centrifuge tube for measurement of radioactivity (PTW Curimentor Model T-12004-0097, Freiburg, Germany), and finally removed from the tube, and affixed to a cardboard platform for imaging.

For multiply-imaged birds, the egg was removed from the sound-isolation chamber under a red photographic safelight, and placed in a small plastic bag (resistant to isoflurane) that was connected by a tube to a volatile anesthesia dispenser at one end, and vented by a tube connected to an absorption filter canister at the other end. Isoflurane mixed with oxygen (initially 1.5 – 2.0%, adjusted down to 0.5-1.0 % after the first 2-3 minutes) was piped through

the bag, and the bag was inserted into the bore of the PET/CT imager. Imaging was conducted at room temperature (28-30° C) in the dark. The purpose of the lower temperature and anesthesia was to abolish the spontaneous movements given by embryos so that clean PET / CT images could be obtained. At the end of imaging, eggs were quickly removed from the imager and the bag under a red photographic safelight, and were placed back on the movement-recording device in the light-tight 37.5° C sound-isolated chamber for approximately 5 minutes to make sure that their heart rates and spontaneous movement recovered to pre-imaging levels. They were then replaced in the light-tight transport container and taken back to their incubator. On the last imaging session, 3 of these embryos were treated exactly like the singly-imaged birds described above.

Although volatile isoflurane anesthesia has been routinely used in animal work, it has been reported to increase apoptosis in the brains of 7-day-old rat pups exposed to it continuously for 6 hrs (61), visible by 2 hrs after the cessation of anesthesia. This can be counteracted by adding xenon to the volatile gas mixture used for anesthesia (62-64). Isoflurane-induced apoptosis is unlikely to have affected glucose uptake in the present studies, because anesthesia was briefly administered after glucose uptake had already taken place.

Potential Effects of Ionizing Radiation from This Experimental Design

Estimation of radiation dosimetry in small laboratory animals is not straightforward. The activity concentration in animal tissues is high since the injected dose does not scale linearly with weight (65), and the small size of the subject allows a larger fraction of the radiation to escape without interacting with body tissues. Since major organogenesis in chicken embryos occurs prior to day 10 of incubation (66), and the earliest radiation exposure we have performed started on day 16 of incubation, teratogenicity is not expected to occur. In terms of absorbed and equivalent doses, we can approximately equate the size and composition of late-stage chicken embryos to a 20 g mouse. In a chicken embryo CT session, the dose deposited in each subject is less than 40 mSv (31). The worst-case scenario would be for animals that underwent multiple CT scans for developmental staging twice a day for five days, so that the total maximum accumulated dose in those animals would be 400 mSv, still well below dose levels that could become worrisome (67,68) or lethal (the LD50/30 = 7 Gy for small rodents (68,69)). A PET tracer injection in a mouse can produce a whole body dose between 6 and 90 cGy (70). In our experiments the dose was not injected into the subject, but rather deposited on top of the inner shell membrane, and this would result in a much lower dose going into the embryo. Therefore, the cumulative exposure to radiation from both the CT and PET procedures as a result of multiple imaging over the last 4-5 days of incubation is compatible with normal development, and the exposure for a single PET/CT imaging session is negligible.

Posthatching Bird Preparation for Imaging

The posthatching birds were used in a preliminary study to examine the feasibility of PET imaging in young chicks. One-to-two-day-old posthatching birds were obtained on their day of hatching and kept in a group in a heated container with free access to food and water prior to imaging. Immediately prior to being introduced singly into a dimly-lit sound-isolation chamber at 32° C, they were injected intramuscularly with 100-280 μCi of 2-deoxy-2-^{18}Fluoro-D-glucose in sterile saline into the body of their breast (pectoralis) muscle. Once in the chamber, they

were exposed to 20 minutes of either the chicken sound (Figure S1B), presented in the same way as in the embryo experiments, or a similar sound constructed from Japanese quail (*Coturnix coturnix japonica*) vocalizations, used in previous experiments (34, 35). After a 20-minute sound exposure period, they were left in silence for a further 10 minutes, then given a lethal overdose of Equithesin anesthesia intramuscularly injected into the pectoralis muscle prior to PET imaging. No CT images were taken of these posthatching animals. Video recordings of the behavior of all individuals revealed that none of them visibly slept during the recording period; they all spent roughly equivalent amounts of time emitting "contact call" vocalizations, and exploring the interior of the chamber.

Behavioral/Cardiac Activity Recording and Analysis

The noninvasive movement-recording device for embryo behavior was based on an earlier design (33) in which three monoaural piezoelectric phonograph cartridges (Fox-Indelson Model 2145-ZST, Madrid) were arranged in a triangle with their styli pointing upwards to hold the egg under study. The egg was positioned (blunt end up) on top of the three styli, which held it in place. The stylus cartridges were connected in parallel; the common signal arising from the three transducers was first amplified with a gain of 60, and then passed through three filtering stages to eliminate electrical interference due to AC power and noise. The first stage was a bandpass filter from 0.05 Hz to 1 KHz used to attenuate both low- and high-frequency noise. The second and the third filtering stages were notch filters, eliminating AC contamination at 50 Hz, and its first harmonic at 100 Hz. The signal was amplified by a factor of 10 between the two notch filters. The output was connected to one channel of a two-channel USB audio digitizer interface (Edirol UA-1A, Los Angeles, CA); a copy of the output to the speaker in the sound-isolation chamber (Figure S1B) was connected to the other channel, so that embryo movement recordings and a record of the stimulation delivered to the embryo were captured simultaneously. Signals were digitized at 44.1 kHz, and were displayed in real time on the computer screen and saved using Audacity v.1.2.6 software (Carnegie Mellon University, Pittsburgh, PA).

Movement recordings were processed using custom-written programs in the SIGNAL digital sound-analysis system. Each recording had any DC offset removed, and a copy was prepared for movement analysis by downsampling (point decimation) by a factor of 10, lowpass filtering at 600 Hz, and resampling to a 2000 Hz sampling rate using cubic spline interpolation. The resulting file is referred to below as the "prepared movement file". A spectrogram of this file was made from 0-30 Hz (discrete Fourier transform (DFT) length 8192 points). Heartbeat activity on these spectrograms consisted of a stack of harmonically-related components at frequencies that were integer multiples of the heart rate; the spectral contour detection algorithm in SIGNAL was used to extract the frequency-time contour of the heartbeat harmonic component with the greatest power. This contour was divided by the harmonic number of the component it was extracted from to yield the fundamental frequency-time contour of the heartbeat, and resampled using cubic spline interpolation to a sampling rate of 2000 Hz. The heart rate – time contour was used to analyze both heart rate changes and the coefficient of variation of the heartbeat.

Another copy of the prepared movement file was processed in two stages to derive an amplitude envelope-time contour for the heartbeat. First, the prepared movement file was

absolute-valued, and visually examined to select a threshold value for the highest-amplitude heartbeat deflection in the recording. An automated program then identified all of the time intervals exceeding this value, and reset them to the value of the highest-amplitude heartbeat value. This altered file was then visually examined to see if there were any remaining portions of the file with lower heartbeat amplitude values that had movement deflections evident, and these portions of the file were reiteratively treated as above until a relatively smooth waveform was obtained for the entire 20 minute recording period. In the second stage, this waveform was smoothed with a 4 sec window and then visually examined after being replotted on top of the original prepared movement file, to make sure that it accurately reflected the amplitude envelope of the heartbeat over the entire recording. Once this fit was satisfactory, an automated program added 10% of the maximum value of this smoothed heart amplitude envelope contour to all of its time points; the result served as a threshold-time contour that had to be exceeded in order for a voltage deflection to be counted as a movement.

A final movement-time contour file was derived by an automated program that took a new copy of the prepared movement file, absolute-valued it, identified time periods that did not exceed their respective values in the threshold-time contour, and set these to zero. Another automated program compiled data on movement bouts and quiescent periods from these final movement-time contours; a quiescent period was defined as an interval between two movements that was $\geq$ 150 msec in duration, and a movement bout consisted of any set of movements separated by less than 150 msec from each other. This program produced a file containing a sequential list of each movement bout and quiescent period duration, and the integrated voltage sum and average voltage/msec (measures of movement size) for each movement bout. An example of an unprocessed egg recording, together with sound stimulation, movement and heartbeat information processed from it are shown in Figure S1C.

Movement and quiescent period bout duration statistics (Figure 4A,B) were calculated by an automated program written in MATLAB (The Mathworks, Natick, MA), which constructed histograms of duration values for each individual recording (quiescent period bins starting from $100*2^n$... msec, where n= 0,1...13, and movement bout bins starting from 0, $100*2^n$... msec, where n = 1,2...13), then calculated the best-fitting exponential and power-law curves for each histogram, and saved the fit statistics and r^2 values into a list file. A fit was declared when one function had significantly ($p < 0.05$) or, in one case, marginally-significantly ($p < 0.06$) better mean fits than the other function AND explained an average of > 90% of the variance. Whenever these conditions were not met, the fit was declared to be indeterminate.

PET/CT Imaging and Image Analysis

Embryos were scanned with the ARGUS PET/CT scanner (30, 31). Samples were located at the center of the field of view (FOV) of the PET system and scanned for 60 minutes with a 400-700 keV energy window. Images were obtained using a 3D-OSEM algorithm with a spatial resolution of 0.7 mm (71). Once the PET scan was over, the bed supporting the sample was automatically moved by a mechanical linear slide to the center of the X-ray computed tomograph (CT) FOV, and was immediately scanned with the tube set at 250 μA and kilovoltages between 35 and 45 keV, depending on the characteristics of the sample. The scanning took nine minutes, and the data were reconstructed using an optimized FDK cone reconstruction (72). The whole process was performed using an integrated console (MMWKS, (54)) that allowed the visualization and

manipulation of the datasets in 3 dimensions, provided analysis tools (segmentation, quantification) as well as visualization tools (registration, multimodality fusion and volumetric rendering), and also provided export and import methods for dataset handling. The console generated intrinsically-registered PET/CT images when both scans were done serially, and also provided co-registration tools based on fiducial marks for manual registration, and based on mutual information (MI) methods for automatic processing (55).

Posthatching animals were scanned with the ATLAS small animal PET scanner (73), and the images were reconstructed by ramp-filtered backprojection from 2D sinograms, with a 3D-OSEM algorithm that achieved an in-plane resolution better than 1.8 mm (74).

CT Image Analysis

CT images were processed for fine-scale developmental staging of the embryos by first removing all extraneous material other than the head from the image (the supporting stage of the imager, the cardboard platform the heads were attached to, any debris) using both user-assisted and automated programs written in ImageJ (U.S. National Institutes of Health, Bethesda, MD). Since the studies were conducted over an extended period of time, there was a possibility that small amounts of drift in CT scanner calibration values could interact with nonlinear developmental changes in the degree of bone calcification to produce unwanted classification errors. For this reason, the thresholding procedure for isolating the skeleton used a proportional criterion based on two reference points, instead of choosing an absolute Hounsfield Unit (HU) value. The HU value for completely mineralized bone in low kilovoltage CT images is at least 10 times larger than muscle tissue, which would be too high to segment the still-calcifying bones of the chicken skull. Setting the threshold to an intermediate level that depended on the actual value of brain/skin/muscle ensured that cartilage was not included, but that more mineralized bone was, and that the level of calcification demanded for inclusion was as uniform as possible across embryos of all ages.

The value for thresholding the skeleton was determined automatically by a program written in ImageJ that made a histogram of the HU values treated as gray levels (256 intensity bins) in the isolated head CT image, and found two points in this histogram: the most common gray level (G_s, which represents the average gray level of brain/skin/muscle tissue), and the maximum value starting from 10 intensity bins above this (G_c, the start of the range where cartilaginous structures began to stand out above brain/skin/muscle tissue). Empirical comparison of the results of different threshold values with the timetable of known calcification events in chick embryo skull development (75-77), and of the head morphology with the standard embryological stages of Hamilton and Hamburger (32), led to the selection of a value = 0.25*(Gs+Gc) for inclusion into the skeleton, which was uniformly applied to all embryos. All points in the CT image above this threshold were set to a value of 1, with all other points set to 0. The resulting image was then filtered (hybrid 3D median filter) and despeckled to remove noise using ImageJ; it is referred to as the “skeletal mask”.

User-assisted programs written in ImageJ and MMWKS were used to make isolated images of two groups of bony structures from the skeletal mask: (a)”vertebral”- the atlas, axis and first three cervical vertebrae, and (b) “basal skull”- the rostroparasphenoid, alaparasphenoid, basiparasphenoid, basioccipital, sphenoid, and exoccipital bones. An automated program written in IDL (ITT Visual Information Solutions, White Plains, NY) was used

to calculate the total volume in mm^3 of each of these bony structure groups. Once all 201 skeletons were processed in this fashion, the basal skull (y-axis) and vertebral (x-axis) values were plotted against each other, and the first principal component was taken. This accounted for 98.5% of the variance in the basal skull-vertebral volume plot; the projection values of each embryo skeleton on the first principal component were used as a measure of developmental stage (Skeletal Age Value, Figure 2A).

PET Image Analysis

Reconstructed PET images were first validated for measurement purposes. The total sum of intensity values in the head on the image was compared to the radioactivity measured in the head immediately prior to imaging by fitting a line to these data with a y-intercept at 0. This was done separately for images collected on different machines, and for images collected on the same machine using different software calibration regimes, yielding a total of four groups of images. The linear fit explained 99.3 % of the variance in one of these cases, and 99.5% of the variance in the three others, demonstrating that the intensity values on the images quantitatively represented the concentration of radioactive glucose in the head of the embryo.

In order to have a common scale of measurement for glucose uptake in brain tissue that would be independent of the total amount of glucose that was made available to the brain, image values were normalized by referencing them to the maximum uptake value found in the pituitary gland, a structure that was clearly visible on all PET images. Maximum values were used because these could be measured automatically in a consistent way, without having to develop criteria for outlining the entire structure to assure equivalent sampling in different embryos. The chick pituitary is connected to the brain, receives a similar blood supply, and is highly metabolically active throughout this period of development (78). A linear regression on log-log coordinates revealed that the maximum pituitary value explained 99.6% of the variance in brain maximum voxel values, with a slope of 1.0. The normalized but spatially untransformed images are referred to below as “normalized reconstructions”.

Brain maxima values were extracted directly from the normalized reconstructions using the segmentation tools in the MMWKS Analysis module. While viewing the 3-D PET image, a threshold was continuously adjusted so as to reveal the cluster of voxels with the highest maximum intensity in the brain / spinal cord rostral to the first cervical vertebra. If this cluster was at or caudal to the rostral pontine reticular formation (rPRF), the threshold was readjusted until a cluster appeared somewhere else in the brain. In order to be counted as a maximum, a volume element (voxel) had to occur as part of a cluster of at least 3 voxels that could be thresholded out from the brain tissue that immediately surrounded them. The position of all such clusters within the nervous system was confirmed by examining their position in a combined CT-PET 3-D image using the “Fused Display” in the MMWKS Registration module.

For other measurements, brains were divided by the developmental stages defined in the text (Ages I, II/III and IV, Figure 2A). Ages II and II were combined to improve statistical power, based on the high similarity of their maximum brain activation patterns (Figure S2B), and because Age III appears to represent the culmination of trends starting in Age II that peak in the population during a brief period just prior to the transition to air-breathing. Age IV was further subdivided into an “early” and “late” stage (with 55 and 54 embryos, respectively). An embryo whose developmental stage was in the center of each of these 5 groups was chosen as

a “standard spatial template” for the group, and the cleaned CT images of the heads of these 5 embryos were put into a standard position and orientation using the “Reformatting Tool” in MMWKS. A custom-written program in IDL that called the library of reformatting tool commands in MMWKS was then used to sequentially align and scale the cleaned head CT image of each embryo to the template CT image for its group in two steps, first using the rigid MI alignment routines of MMWKS, and then using the rigid-plus-scaling alignment, and storing a file containing the spatial transformation values. All alignments were checked visually using the “Fused Display” in the MMWKS Registration module and modified if necessary. Alignment transformations were also calculated among sequential pairs of the standard spatial templates for these groups.

Once these alignments had been obtained for all embryos, the spatial transformation values were used to align all of the normalized PET images, which are referred to below as “spatially-aligned PET images”. For the 16 posthatching birds, the bird with the brain of median size was chosen, and its brain was aligned to the spatially-aligned PET image of the “late stage” Age IV standard using the same procedure as above; the other 15 posthatching birds were then aligned to it. A template for the whole brain was created for each group by making a mean PET image from the spatially-aligned PET images of all birds in the group (to average out individual variation), and this mean image was then thresholded at the lowest value for which all brain structures were included in the masks for all developmental groups (= 105 normalized units). The skull CT image of the standard template was then used to mask out any areas that were not within the skull. These “whole-brain” templates were used for the measurements illustrated in Figure S1D (the basis for assigning glucose activation pattern designations), and for measuring the distribution of brain glucose uptake values shown in Figures 2B, and Figures S2B and S3B,C. These measurements were captured using custom-written programs in IDL.

Measurements of the regions of interest (ROIs) shown in Figure 2B used the spatially-aligned PET images. The ROIs were created using the mean spatially-aligned PET image from Age II/III; the rPRF ROI was created by thresholding this image at a value of 125 normalized units and masking all activations outside the rPRF; the MRF ROI was created by subtracting the mean spatially-aligned PET images of the rInactive embryos from those of the pActive embryos and masking all activations that were below zero or clearly outside the mesencephalic reticular formation. These ROIs were then spatially transformed to the other groups so that a common set of ROIs was used for all measurements.

For measuring volumes of activation within 15% of the brain maximum (Figures S2B and S3C), the normalized reconstructions were used to produce spatial masks of these regions by thresholding at 0.85 of the maximum value above the rPRF, and removing any areas that were outside of the skull. These masks were then spatially transformed to their developmental stage standards using the spatial transformation values described above.

Eye (iris) muscle and jaw (mandibular depressor) muscle activations (Figure 4C,D) were measured from the normalized reconstructions for each embryo. The eye value was derived by taking the mean value of all voxels with an intensity $\geq$ 50 normalized units bilaterally in the region bounded 3-dimensionally by the iris ring bones, which were visible in the CT images of all embryos. The mandibular depressor muscle was also visible bilaterally in all embryos as two discrete spheres of activation on each PET image; these were demarcated using the “Region

Growing" tool in the MMWKS Analysis module with a threshold of 70 and seeds placed on the center of the activation for each muscle. The bilateral average of the intensity values was used.

Statistical Tests

This study was designed to examine large-scale pattern changes in glucose uptake over all ages and stimulus conditions. Because of the large degree of variation in overall glucose uptake levels and the "patchy" spatial distribution of high-uptake areas in the brains studied here, the PET data set as a whole did not meet the assumptions required for applying statistical parametric mapping techniques (SPM, 79). Instead of applying the extensive spatial smoothing required to make these data suitable for SPM, we applied standard statistical analyses using measurements taken on unsmoothed data.

All statistical comparisons used nonparametric statistical tests corrected for multiple comparisons (all p-values were two-tailed). Frequency comparisons were done using the G-test, corrected for continuity with the Williams correction (80), except in cases where one of the categories had zero frequency, in which case Fisher's exact tests (80) were used. Log-linear analysis (80) was used to analyze 3-way frequency data (Figure 5C). These frequency analyses were conducted using BIOMstat (Exeter Software, Setauket, NY). Nonparametric 2-way analysis of variance (used to analyze the Age II/III data in Figure 4D) was conducted according to the Scheirer-Ray-Hare extension of the Kruskal-Wallis test (80). Kruskal-Wallis one-way analysis of variance with post-hoc tests corrected for multiple comparison (75) were carried out in Statview 5 (SAS, Cary, NC) and Matlab, as were correlations, partial correlations, Mann-Whitney tests (81), and Wilcoxon matched-pair sign-rank tests (81). For all correlations, both Pearson product-moment (r) and Spearman rank correlations (ρ) were calculated, and both the magnitude and significance of these tests agreed with each other; the Pearson values are reported here.

Supplemental References

56. Jacob, S.W., and de la Torre, J.C. (2009) Pharmacology of dimethyl sulfoxide in cardiac and CNS damage. Pharmacol. Rep. 61, 225-235.

57. DiGiorgio, A.M., Hou, Y., Zhao, X., Zhang, B., Lyeth, B.G., and Russell, M.J. (2008) Dimethyl sulfoxide provides neuroprotection in a traumatic brain injury model. Restor. Neurol. Neuros. 26, 501-507.

58. Qi, W., Ding, D., and Salvi, R.J. (2008). Cytotoxic effects of dimethyl sulfoxide (DMSO) on cochlear organotypic cultures. Hearing Res. 236, 52-60.

59. Götte, M., Hofmann, G., Michou-Gallani, A.I., Glickman, J.F., Wishart, W., and Gabriel, D. (2010) An imaging assay to analyze primary neurons for cellular neurotoxicity. J. Neurosci. Meth. 192, 7-16.

60. Hanslick, J.L., Lau, K., Noguchi, K.K., Olney, J.W., Zorumski, C.F., Mennerick, S., and Farber, N.B. (2009) Dimethyl sulfoxide (DMSO) produces widespread apoptosis in the developing central nervous system. Neurobiol. Dis. 34, 1-10.

61. Jevtovic-Todorovic, V., Hartman, R.E., Izumi, Y., Benshoff, N.D., Dikranian, K., Zorumski, C.F., Olney, J.W., and Wozniak, D.F. (2003) Early exposure to common anesthetic agents causes widespread neurodegeneration in the developing rat brain and persistent learning deficits. J. Neurosci. 23, 876-882.

62. Ma, D., Williamson, P., Januszewski, A., Nogaro, M.C., Hossain, M., Ong, L.P., Shu, Y., Franks, N.P., and Maze, M. (2007). Xenon mitigates isoflurane-induced neuronal apoptosis in the developing rodent brain. Anesthesiology 106, 746-753.

63. Cattano, D., Williamson, P., Fukui, K., Avidan, M., Evers, A.S., Olney, J.W., and Young, C. (2008) Potential of xenon to induce or to protect against neuroapoptosis in the developing mouse brain. Can. J. Anesth. 55, 429-436.

64. Shu, Y., Patel, S.M., Pac-Soo, C., Fidalgo, A.R., Wan, Y., Maze, M., and Ma, D. (2010) Xenon pretreatment attenuates anesthetic–induced apoptosis in the developing brain in comparison with nitrous oxide and hypoxia. Anesthesiology 113, 360-368.

65. Jagoda, E.M., Vaquero, J.J., Seidel, J., Green, M.V., and Eckelman, W.C. (2004) Experiment assessment of mass effects in the rat: implications for small animal PET imaging. Nucl. Med. Biol. 31, 771-779.

66. Romanoff, A.L. (1960) The Avian Embryo: Structural and Functional Development (New York: Macmillan).

67. Malladi, S.M., Bhilwade, H.N., Khan, M.Z., and Chaubey, R.C. (2007) Gamma ray induced genetic changes in different organs of chick embryo using peripheral blood micronucleus test and comet assay. Mutat. Res. 630, 20–27.

68. Ford, N.L., Thornton, M.M., and Holdsword, D.W. (2003) Fundamental image quality limits for microcomputed tomography in small animals. Med. Phys. 30, 2869–2877.

69. Obenaus, A., and Smith, A. (2004) Radiation dose in rodent tissues during micro-CT imaging. J. X-Ray Sci. Technol. 12, 241–249.

70. Hildebrandt, I.J., Su, . I. J., and Weber, W.A. (2008) Anesthesia and other considerations for in vivo imaging of small animals. ILAR J. 49, 17-26.

71. Herráiz, J.L., España, S., Vaquero, J.J., Desco, M., and Udías, J.M. (2006) FIRST: Fast iterative reconstruction software for (PET) tomography. Phys. Med. Biol. 51, 4547-4565.

72. Abella, M., Vaquero, J.J., Sisniega, A., Pascau, J., Udías, J.M., García, V., Vidal, I., and Desco, M. (2011) Software architecture for multi-bed FDK-based reconstruction in x-ray CT scanners. Comput. Meth. Prog. Bio., in press, 1-15, http://dx.doi.org/10.1016/j.bbr.2011.03.031.

73. Seidel, J., Vaquero, J.J., and Green, M.V. (2003) Resolution uniformity and sensitivity of the NIH ATLAS small animal PET scanner: Comparison to simulated LSO scanners without depth-of-interaction capability. IEEE T. Nucl. Sci. 50, 1347-1350.

74. Johnson, C.A., Seidel, J., Carson, R.E., Gandler, W.R., Sofer, A., Green, M.V., and Daube-Witherspoon, M.E.(1997) Evaluation of 3D reconstruction algorithms for a small animal PET camera. IEEE T. Nucl. Sci. 44, 1303-1308.

75. Parker, W.M. (1869) On the structure and development of the skull of the common fowl (Gallus domesticus). Philos. T. Roy. Soc. 159, 755-807.

76. Jollie, M.T. (1957) The head skeleton of the chicken and remarks on the anatomy of this region in other birds. J. Morphol. 100, 389-436.

77. Hogg, D.A. (1990) The development of pneumatisation in the skull of the domestic fowl (Gallus gallus domesticus). J. Anat. 169, 139-151.

78. Parkinson, N., Collins, M.M., Dufresne, L., and Ryna, A.K. (2010) Expression patterns of hormones, signaling molecules, and transcription factors during adenohypothesis development in the chick embryo. Dev. Dynam. 239, 1197-1210.

79. Friston, K.J., Ashburner, J.T., Kiebel, S.J., Nichols, T.E., and Penny, W.D. (2007) Statistical Parametric Mapping: The Analysis of Brain Functional Images, (New York: Academic Press).

80. Sokal, R.R., and Rohlf, F.J. (1995) Biometry: The principles and practice of statistics in biological research, 3rd Edition, (New York: Freeman).

81. Siegel, S., and Castellan, N.J. Jr. (1988) Nonparametric Statistics for the Behavioral Sciences, 2nd Edition, (New York: McGraw-Hill).